NASA TM-87576

NASA Technical Memorandum 87576

A Preliminary Evaluation Of A Failure Detection Filter For Detecting And Identifying Control Element Failures In A Transport Aircraft

W. Thomas Bundick

July 1985

National Aeronautics and
Space Administration

Langley Research Center
Hampton, Virginia 23665

SUMMARY

A failure in an aircraft control element must be accommodated in near real time by the pilot and/or automatic control system in order to prevent a possibly tragic accident. A first step in this accommodation is the detection and identification of the failure. This report presents the results of an evaluation of the failure detection filter for the detection and identification of control element failures in transport aircraft.

With the failure detection filter the vector of filter residuals for a given actuator type failure maintains a prescribed direction in measurement space. A residual processor, such as the correlator and threshold detector described in this work, can be used to detect the occurrence of a failure and to identify the failure. Such a failure detection filter was evaluated using a digital computer linear simulation of the longitudinal dynamics of a B-737 aircraft. The simulation included sensor errors and wind turbulence.

With the thresholds set at a level determined by heavy clear air turbulence, approximately one half of the failures in the elevator, throttle, stabilizer, and spoiler were successfully detected. However, in heavy clear air turbulence and in thunderstorm turbulence all of the failures were detected, while in lesser turbulence none were detected. The primary reason for the missed detections at the lower turbulence levels was the necessity to set the thresholds sufficiently high to avoid false alarms in heavy turbulence during which the residual levels are increased.

With some measurements, such as the acceleration measurements in this system, some actuator type failures feed directly into the measurement equation with the result that the filter residuals from these failures cannot be confined to a constant direction in measurement space. Also, with the state space formulation used in this evaluation a steady state wind affects the filter residuals in the same way as does an actuator type failure.

From the results of the simulation runs, it is concluded that false alarms/missed detections due to wind turbulence are a significant problem which must be overcome before the failure detection filter and correlation processor can be used to detect and identify control element failures in transport aircraft.

INTRODUCTION

For certain anticipated failures in transport aircraft operations there are established procedures for the pilot to follow. A typical example is the procedure for handling an engine outage during takeoff. There are, however, unanticipated failure modes for which no appropriate emergency procedures will be available. These unanticipated failures must be handled by the pilot and/or the automatic control system in real time to decrease the probability of a tragic accident.

In the case of a hard-over failure in a control element, the pilot may have only a matter of seconds to take corrective action before the aircraft reaches an irrecoverable condition. In the case of a failure of lesser magnitude the pilot may have more time to take corrective action, but the failure and, hence, the proper

corrective action may be difficult to identify. In either case the pilot may require assistance from the aircraft systems to help him take the appropriate corrective action in a timely manner.

A considerable amount of work has been done in the area of failure detection and identification (FDI) in dynamic systems, and Willsky has provided a well known survey of many of the available FDI techniques (ref. 1). Chow (ref. 2) and Willsky and Chow (ref. 3) have examined the problem of generating residuals from the system measurement data for use in decision making processes to detect and identify failures. The detection of failures in sensors has been investigated by several authors, including Motyka, et al. (ref. 4); Deyst, et al. (ref. 5); Caglayan (ref. 6); and Friedland (ref. 7). The Generalized Likelihood Ratio has been investigated for FDI applications by Willsky and Jones (ref. 8); Chow, Dunn, and Willsky (ref. 9); Bueno, et al. (ref. 10); Bueno (ref. 11); MIT (ref. 12); Liu and Jones (ref. 13); and Chang and Dunn (ref. 14). The technique has been exercised in a simplified simulation of the F-8 aircraft dynamics by Bueno and others at MIT (refs. 9-12), and Tylee (ref. 15) has examined the use of the GLR to detect failures in a nuclear reactor. Another FDI technique is the failure detection filter (FDF). Beard (ref. 16) developed the theory of the failure detection filter for linear deterministic continuous systems using a matrix algebra approach. Jones (ref. 17) extended this theory to stochastic and sampled data systems using a vector space approach. Messerole (ref. 18) has applied the failure detection filter to the problem of detecting and identifying failures in an F100 engine.

This report presents the results of an evaluation of the capabilities of the failure detection filter for the detection and identification of control element failures in a transport aircraft. This evaluation was conducted primarily by implementing the failure detection filter in a linear simulation of the longitudinal dynamics of a B-737 aircraft and examining the performance of the filter in detecting step failures in the elevator, throttle, stabilizer, or spoilers. The text includes a development of the theory of the failure detection filter for fully measured systems, a brief discussion of the aircraft simulation and the filter implementation, a presentation and discussion of the results, and conclusions. The aircraft simulation is discussed in detail in appendix A. The preprocessor used to transform the measurements into a form suitable for use by the failure detection filter is discussed in appendix B.

SYMBOLS

A	system transition matrix
A_W	wind system transition matrix
A_{x_b}, A_{z_b}	acceleration in the x-, z-direction (body axes), ft/sec (sub-subscript s denotes stability axes)
B	control input matrix
B_i	i-th column of B
B_W	wind system plant noise input matrix
b	wing span, ft

$b(\cdot)$	measurement bias error
C_W	transformation matrix relating W to w and W_k to w_k
c_j	correlation of filter residual with j-th output failure vector
c'_j	correlation c_j normalized by multiplication by $(1 - \lambda)/\lvert Hf_j \rvert$
c''_j	normalized correlation used in computing estimate of the failure magnitude
c^*_j	correlation c'_j normalized by division by threshold ε_j
$_N c^*_j$	correlation c^*_j averaged over an N-sample data window
D	plant noise input matrix; failure detection filter gain
F	covariance matrix of the wind system plant noise ξ
f_i	failure vector
$G_{\cdot}(s)$	filter transfer function
H	observation matrix
H_F	model of the observation matrix used in the filter
h	altitude, ft
I	identity matrix
i	index denoting the i-th failure vector from the set of constrained failure vectors
k	sample number
$L_u, L_w,$	turbulence scales in the x- and z-directions, respectively, ft
q	perturbed inertial pitch rate, rad/sec
q_k	filter error vector
q_W	pitch rate due to wind, that is, rotation of the atmosphere about the y-axis, rad/sec
$_N R_k$	vector of filter residuals averaged over an N-sample data window
R_η	covariance matrix of the plant noise η_k
R_ξ	covariance matrix of the wind system plant noise ξ_k
r_k	vector of filter residuals
r_{ss}	vector of steady state filter residuals

$S_u(\cdot), S_\alpha(\cdot), S_q(\cdot)$ power spectral density of the x-, angle-of-attack, and pitch rate-components, respectively, of the wind turbulence

t time, sec

t_k time at k-th sample, sec

U_o trim inertial velocity in x-direction, ft/sec

u, u_k control vector

$u_k(\cdot)$ components of control vector u_k

$u(0)$ steady state wind in the x-direction, ft/sec

u' perturbed inertial speed in the x-direction normalized by the trim velocity U_o

u'_w normalized speed in the x-direction due to wind, that is, normalized wind velocity in the negative x-direction

u'_g, u'_s gust and steady state components, respectively, of u'_w

V_a airspeed, ft/sec

v_k observation, or sensor, noise vector

W, W_k wind system state vector

$W(\cdot)$ components of wind system state vector W_k

w, w_k wind, or plant noise, vector

$w_s(0)$ steady state wind in the z-direction, ft/sec

x, x_k system state vector

$x_k(\cdot)$ component of system state vector x_k

$\hat{x}_k$ estimate of the state vector x_k

y_k in general, the observation, or measurement, vector; for the B-737 simulation, the vector of pseudo-measurements after preprocessing

$\hat{y}_k$ value of the observation vector, or pseudo-measurement vector, predicted by the filter

z, z_k measurement vector from simulation prior to preprocessing

$z_k(\cdot)$ component of the observation vector z_k

α, α_k failure magnitude; perturbed inertial angle-of-attack, rad

α_w part of the angle-of-attack due to winds, rad

α_g, α_s gust and steady state components, respectively, of α_w, rad

α_o trim value of the angle-of-attack, rad

Γ disturbance transition matrix

Γ_H matrix coupling control element failure into the measurement equation

Γ_w disturbance transition matrix for the wind input w_k and defined by equation (A55)

δ_e perturbed elevator position, deg

δ_{jk} unit impulse function

δS perturbed stabilizer position, deg

δsp perturbed spoiler position, deg

δst perturbed stabilizer command, deg

δT perturbed thrust, klbs

δth perturbed throttle command, deg

ε_j detection threshold for correlation c'_j

η_k wind disturbance vector defined by equation (A56)

θ failure time, or sample number; perturbed pitch, rad

θ_o trim value of pitch, rad

θ_{ij} angle between output event vectors Hf_i and Hf_j

λ filter eigenvalue

ξ, ξ_k wind system plant disturbance vector

σ_u, σ_w RMS velocities of wind turbulence in the x- and z-directions, respectively, ft/sec

τ time, sec

ϕ system state transition matrix

ϕ_F filter state transition matrix

ϕ_W wind system state transition matrix

ψ control transition matrix

ψ_F filter control transition matrix

ψ_i i-th column of ψ

Ω spatial frequency, rad/ft

ω temporal frequency, rad/sec

Notation:

$\hat{}$ indicates estimated value

F superscript F indicates that the variable is used in the filter formulation

T superscript T denotes transpose

$E\{\cdot\}$ expectation operator

$\langle \cdot, \cdot \rangle$ vector inner product

$| \; |$ vector magnitude

Acronyms:

CAT Clear Air Turbulence

FDF Failure Detection Filter

FDI Failure Detection and Identification

GLR Generalized Likelihood Ratio

RMS Root-Mean-Square

FAILURE DETECTION FILTER THEORY

A failure detection filter (FDF) is a tracking filter, or state estimator, designed to assist in the detection and identification of a failure in a linear system by selecting the filter feedback gains such that the filter residuals always lie in a constant direction for a given failure (lie in a plane rather than a constant direction for most sensor failures). The work by Beard (ref. 16) and Jones (ref. 17) was devoted to proving the existence of such a filter under certain conditions and to developing a procedure for accomplishing the filter design.

The failure detection filter differs from many other tracking filters, such as the Kalman Filter, in the following way: although the failure detection filter is a state estimator, it is not designed primarily to minimize the tracking, or estimation, error, and therefore its estimation accuracy is not normally as good as a Kalman Filter. As an FDI technique, it differs from the Kalman Filter/Generalized Likelihood Ratio approach in that the FDF design does not depend on the time history of the failure magnitude as does the GLR. In other words, for a given failure type (direction in state space), the FDF design is independent of whether the failure amplitude is a step function, a ramp, or some other function of time. As an FDI tool the primary purpose of the FDF is to generate a vector sequence of residuals which must then be processed by decision making algorithms to declare the presence of a failure (detection) and to declare the type of failure (identification). These

decision algorithms may depend on the expected variation of the failure magnitude with time.

Beard and Jones have developed the failure detection filter theory for a general linear system, but the theory for a fully measured system is considerably simplified. A fully measured system is defined as a system for which the number of independent measurements is equal to the number of system states, that is, $r_k(H) = n$. The aircraft system investigated in this work is a fully measured system.

Consider a noise free, linear, time-invariant, fully measured system with a failure described by the equations

$$x_{k+1} = \phi x_k + \psi u_k + \alpha_k f_i; \qquad i = 1,2,\ldots,L \tag{1}$$

$$y_{k+1} = Hx_{k+1} \tag{2}$$

where

x_k = n-dimensional state vector

y_k = m-dimensional observation, or measurement, vector

u_k = r-dimensional control vector

f_i = n-dimensional failure vector describing the direction of the failure in state space

i = index denoting the i-th failure from a set of L possible failures

α_k = failure magnitude

ϕ = nxn state transition matrix

ψ = nxr control transition matrix

H = mxn observation, or measurement, matrix

A failure of a control element such as an actuator can be described by this model. For example, suppose that in this system the i-th element of u_k were the control input in degrees to an actuator. Then the failure vector f_i for this actuator would be the i-th column of ψ, and α_k would be the magnitude of the failure in degrees. Many changes in plant dynamics also can be represented using the model in equation (1). Sensor failures require a different model and are not treated in this report.

A failure detection filter designed for such a system is described by

$$\hat{x}_{k+1} = \phi\hat{x}_k + \psi u_k + D(y_k - \hat{y}_k) \tag{3}$$

$$\hat{y}_{k+1} = H\hat{x}_{k+1} \tag{4}$$

where

$\hat{x}_k$ = estimated n-dimensional state vector

$\hat{y}_k$ = predicted m-dimensional observation vector

D = filter gain

Define the filter error vector q_k as follows:

$$q_k = x_k - \hat{x}_k \tag{5}$$

From equations (1) through (4) the dynamics of the error are described by

$$\begin{aligned} q_{k+1} &= \phi(x_k - \hat{x}_k) - D(y_k - \hat{y}_k) + \alpha_k f_i \\ &= (\phi - DH)q_k + \alpha_k f_i \end{aligned} \tag{6}$$

The solution to equation (6) is

$$q_{k+1} = (\phi - DH)^{k+1} q_o + \sum_{j=0}^{k} (\phi - DH)^{k-j} \alpha_j f_i \tag{7}$$

where q_o is the initial condition of q_k. Since the true system state x_k is unknown, this error is unobservable. However, the residual r_k, defined by equation (8) is observable.

$$\begin{aligned} r_k &= y_k - \hat{y}_k \\ &= Hq_k \\ &= H(\phi - DH)^k q_o + H \sum_{j=0}^{k-1} (\phi - DH)^{k-j-1} \alpha_j f_i \end{aligned} \tag{8}$$

In general, the direction of r_k continually changes in residual space with time (sample number k) because of the repeated multiplication of the failure vector f_i by the matrix $(\phi - DH)$.

Now let

$$\phi - DH = \lambda I \tag{9}$$

where the λ's are the n eigenvalues of the matrix $(\phi - DH)$. Then equation (8) becomes

$$r_k = \lambda^k H q_o + H \sum_{j=0}^{k-1} \lambda^{k-j-1} \alpha_j f_i \tag{10}$$

For a stable filter, λ is less than 1. Now as k increases, the transient term resulting from the initial condition approaches zero, and the residual becomes

$$r_k \cong H \sum_{j=0}^{k-1} \lambda^{k-j-1} \alpha_j f_i$$

$$= \sum_{j=0}^{k-1} \lambda^{k-j-1} \alpha_j H f_i \qquad \text{for large } k \tag{11}$$

Note that after the initial transient has decayed, the residual is always in the direction Hf_i as was desired. If the failure magnitude α_k is a constant α, then the residual approaches a steady state magnitude as well as direction.

$$r_{ss} = \frac{\alpha H f_i}{1 - \lambda} \tag{12}$$

From equation (9) the filter gain is found to be

$$D = (\phi - \lambda I) H^{-1} \qquad \text{for } m = n \text{ and } r_k(H) = n \tag{13}$$

$$D = (\phi - \lambda I)(H^T H)^{-1} H^T \qquad \text{for } m > n \text{ and } r_k(H) = n \tag{14}$$

Equations (3) through (14) define the failure detection filter which will produce a vector sequence of residuals r_k. We now need a technique, or algorithm, for processing the residuals in order to detect the presence of a failure and to identify the failure. One of the simplest techniques would be to correlate the residuals with each of the output failure vectors Hf_j and to select the vector $f_{\hat{i}}$ corresponding to the largest correlation as the failure and to declare a failure if the correlation exceeds a threshold. Let the correlation be defined as

$$c_j = \langle Hf_j, r_k \rangle \tag{15}$$

where $\langle \cdot, \cdot \rangle$ denotes the inner product. Substituting the steady state value for the residual from equation (12), the correlation becomes

$$c_j = \langle Hf_j, Hf_i \rangle \frac{\alpha}{1 - \lambda} \tag{16}$$

Using this technique, a mis-identification would occur if the failure vectors were such that $\langle Hf_j, Hf_i \rangle$ exceed $\langle Hf_i, Hf_i \rangle$. To avoid this difficulty, use the correlation defined by

$$\begin{aligned} c'_j &= \langle Hf_j, r_k \rangle \frac{(1 - \lambda)}{|Hf_j|} \\ &= \langle Hf_j, Hf_i \rangle \frac{\alpha}{|Hf_j|} \\ &= |Hf_i| \alpha \cos \theta_{ji} \end{aligned} \tag{17}$$

where θ_{ji} = angle between the vectors Hf_j and Hf_i. Once the c'_j, $j = 1,2,\ldots,L$, are computed, the failure is identified as that vector corresponding to the largest normalized correlation, that is

$$\hat{i} = \arg \max_j c'_j \tag{18}$$

A failure is declared if and only if the correlation exceeds a threshold determined a priori by analysis and experiment, that is, if $c_{\hat{i}} > \varepsilon_{\hat{i}}$.

If a failure is declared, the failure magnitude can be estimated using a different normalization of the correlation as follows:

$$\hat{\alpha} = c''_{\hat{i}}$$

$$= \langle Hf_{\hat{i}}, r_k \rangle \frac{(1 - \lambda)}{|Hf_i|^2} \tag{19}$$

Note that

$$\hat{\alpha} = \frac{|Hf_{\hat{i}}| \cdot |Hf_i|}{|Hf_{\hat{i}}|^2} \alpha \cos \theta_{\hat{i}i}$$

$$= \alpha \quad \text{if} \quad \hat{i} = i \tag{20}$$

When the system includes plant noise (wind gusts) and sensor noise, the correlations will be random variables. Therefore, in a practical application a method is needed to reduce the variance of the correlations and thus reduce the false alarms, missed detections, and failure mis-identifications. Perhaps the simplest method is to average the correlations over a window of N data points, or residuals. The averaged correlation becomes

$${}_N c'_j = \langle Hf_j, {}_N R_k \rangle \frac{(1 - \lambda)}{|Hf_j|} \tag{21}$$

where

$${}_N R_k = \frac{1}{N} \sum_{n=1}^{N} r_{k-n+1} \tag{22}$$

The estimates $\hat{i}$ and $\hat{\alpha}$ are computed as in equations (18) and (19) using ${}_N c'_j$ and ${}_N R_k$ in place of c'_j and r_k, respectively.

Note from equation (17) that in the absence of noise the correlations c'_i and c'_j differ by the factor $\cos \theta_{ij}$. Thus the angle between the output failure vectors is a measure of the ease with which the failures can be correctly identified.

EVALUATION OF THE FAILURE DETECTION FILTER VIA SIMULATION

The Aircraft Simulation

To achieve the objective of obtaining a preliminary evaluation of the capability of the failure detection filter to detect and identify failures in an aircraft control system, the filter was implemented in a digital computer linear simulation of the longitudinal dynamics of a B-737 aircraft using a small perturbation model. These dynamics are described in state space by the equation

$$x_{k+1} = \phi x_k + \psi u_k + \Gamma w_k + \alpha_k f_i + \eta_k \tag{23}$$

The aircraft state vector is defined by

$$x_k = \begin{bmatrix} x_k(1) \\ x_k(2) \\ x_k(3) \\ x_k(4) \\ x_k(5) \\ x_k(6) \end{bmatrix} = \begin{bmatrix} \theta \\ u' \\ \alpha \\ q \\ \delta T \\ \delta S \end{bmatrix} \tag{24}$$

where

θ = pitch attitude

u' = normalized speed in the x-direction

α = angle-of-attack

q = pitch rate

δT = thrust

δS = stabilizer position

The control vector is defined by

$$u_k = \begin{bmatrix} u_k(1) \\ u_k(2) \\ u_k(3) \\ u_k(4) \end{bmatrix} = \begin{bmatrix} \delta_e \\ \delta th \\ \delta st \\ \delta sp \end{bmatrix} \tag{25}$$

where

δ_e = elevator command (= elevator position)

δth = throttle command

δst = stabilizer command

δsp = spoiler command (= spoiler position)

The plant noise vectors w_k and η_k represent the winds and will be discussed later. The state transition matrix ϕ, the control transition matrix ψ, and the disturbance transition matrix Γ were derived from the continuous time system matrices A, B, and D, respectively. The system matrices A, B, and D were computed from data supplied by the aircraft manufacturer for various aircraft trim conditions. All of the results discussed in this report were obtained for the aircraft trimmed for final approach with the exception of a few simulation runs to evaluate the effects of modeling errors.

To evaluate the performance of the failure detection filter four types of failures with three magnitudes for each type were simulated. These four types were step failures in the elevator, throttle, stabilizer, and spoiler. The failure vectors were derived from the control transition matrix for a step change of unity magnitude, for example for an elevator position change of one degree. The three magnitudes were chosen to represent a hard-over failure, a soft failure, and a failure of intermediate magnitude. The failure types and magnitudes are listed in table I. Of course, these vectors change as the ψ-matrix changes with the aircraft trim conditions.

TABLE I.- FAILURE TYPES AND MAGNITUDES

Failure	
Type	Magnitude
Elevator	10°, 3°, 1°
Throttle	40°, 12°, 4°
Stabilizer	-6°, 3°, -1°
Spoiler	8°, 3°, 1°

The Wind Simulation

To provide a realistic wind environment for evaluation of the failure detection filter the simulation included both turbulence, or gusts, and steady state winds. The gust components in normalized x-velocity, angle-of-attack, and pitch rate were modeled using the familiar Dryden spectra (ref. 19), which are

$$S_u(\Omega) = \frac{2\sigma_u^2 L_u}{1 + (L_u \Omega)^2} \tag{26}$$

$$S_{\alpha}(\Omega) = \frac{\sigma_w^2 L_w}{V_a^2} \cdot \frac{1 + 3(L_w\Omega)^2}{\left[1 + (L_w\Omega)^2\right]^2} \tag{27}$$

$$S_q(\Omega) = \frac{\Omega^2 V_a^2}{1 + (4b\Omega/\pi)^2} \cdot S_{\alpha}(\Omega) \tag{28}$$

where

Ω = spatial frequency, ft

b = wing span
= 93 ft

V_a = aircraft airspeed, ft/sec
= 216 ft/sec in the landing configuration simulated

L_u, L_w = turbulence scales in the x- and z-directions, respectively
= 1750 ft

σ_u, σ_w = rms velocities of turbulence in the x- and z-directions, respectively, ft/sec

After conversion from the frequency domain to the continuous time domain in state space followed by conversion to discrete time, the state equations for the wind system become

$$W_{k+1} = \phi_W W_k + \xi_k \tag{29}$$

where

W_k = 6-dimensional wind state vector with $W_k(5)$ and $W_k(6)$ being the steady state components in angle-of-attack and normalized x-velocity, respectively

ϕ_W = wind state transition matrix

ξ_k = zero mean, white, Gaussian random vector sequence

In order to provide a thorough evaluation of the FDF, a wide range of wind conditions were included in the simulation runs. RMS turbulence velocities corresponding to medium and heavy clear air turbulence (CAT) and to thunderstorm conditions were simulated together with steady state winds. Calm (no wind/turbulence) conditions were also simulated. These conditions were summarized in table II.

TABLE II.- WIND CONDITIONS USED IN THE SIMULATION

Turbulence conditions	RMS gust velocity, ft/sec		Steady state wind, ft/sec	
	σ_u	σ_w	$u_s(0)$	$w_s(0)$
None	0	0	0	0
Medium	2.7	2.7	10	0
Heavy	7.0	7.0	10	0
Thunderstorm	21.0	21.0	10,39	0

The Measurements

To enhance the capability to solve the FDI problem it was desired to provide a rather complete set of measurements for input to the failure detection filter. On the other hand, for the evaluation results to be credible, the measurement set must be technologically feasible, if not typical, for a modern day transport aircraft. The measurements selected for inclusion in the simulation are pitch attitude, x- and z-accelerations, pitch rate, airspeed, altitude rate, and angle-of-attack. The measurements formed a 7-dimensional measurement vector z_k defined by

$$z_k = \begin{bmatrix} z_k(1) \\ z_k(2) \\ z_k(3) \\ z_k(4) \\ z_k(5) \\ z_k(6) \\ z_k(7) \end{bmatrix} = \begin{bmatrix} f_1(\theta) \\ f_2(A_{x_b}) \\ f_3(A_{z_b}) \\ f_4(q) \\ f_5(V_a) \\ f_6(\dot{h}) \\ f_7(\alpha) \end{bmatrix} \tag{30}$$

The measurements $z_k(1)$ - $z_k(7)$ include errors such as noise, bias, scale factor, and misalignment where appropriate. Numerical values for the errors are listed in table A.1.

The FDF requires measurements that are linear functions of the state variables, that is, measurements that can be related to the state variables via the measurement matrix H_F. The measurements z_k described by equation (30) do not meet this requirement since many of the functional relationships are non-linear. To circumvent this difficulty a pre-processor was used to transform the measurement vector into a vector of pseudo-measurements, or observations, y_k which could be approximated as linear functions of the states. A detailed description of the pre-processor and the H_F-matrix can be found in appendix B.

The Filter

A 6-state failure detection filter was designed and implemented in the aircraft simulation for evaluation. The model of the B-737 aircraft used to design the filter is described by the equation

$$x_{k+1} = \phi_F x_k + \psi_F u_k + \alpha_k f_i^F; \qquad i = 1,\ldots,4 \tag{31}$$

The aircraft states and controls are the same as those used in the simulation.

$$x_k = \begin{bmatrix} x_k(1) \\ x_k(2) \\ x_k(3) \\ x_k(4) \\ x_k(5) \\ x_k(6) \end{bmatrix} = \begin{bmatrix} \theta \\ u' \\ \alpha \\ q \\ \delta T \\ \delta S \end{bmatrix} \tag{32}$$

where

θ = pitch attitude

u' = normalized speed in the x-direction

α = angle-of-attack

q = pitch rate

δT = thrust

δS = stabilizer position

$$u = \begin{bmatrix} u_k(1) \\ u_k(2) \\ u_k(3) \\ u_k(4) \end{bmatrix} = \begin{bmatrix} \delta_e \\ \delta th \\ \delta st \\ \delta sp \end{bmatrix} \tag{33}$$

where

δe = elevator command (= elevator position)

δth = throttle command

δst = stabilizer command

δsp = spoiler command (= spoiler position)

The state transition matrix ϕ_F and the control transition matrix ψ_F are derived from the continuous time aircraft system matrices as discussed in appendix A, but they are designated with a subscript F to emphasize that the model used in the filter may be inaccurate and may differ from the matrices ϕ and ψ describing the actual aircraft (simulation). The effect of such inaccuracies have been explored briefly and are discussed in the results section.

The failure vectors f_i^F correspond to failures in the elevator, throttle, stabilizer, and spoiler. The superscript F is used to denote that the vectors in the model are derived from the model control transition matrix ψ_F and may differ from the failure vectors used in the simulation.

Using the model just discussed the FDF is described by the equations

$$\hat{x}_{k+1} = \phi_F \hat{x}_k + \psi_F u_k + D(y_k - \hat{y}_k) \tag{34}$$

$$\hat{y}_{k+1} = H_F \hat{x}_{k+1} \tag{35}$$

The filter gain was computed from

$$D = (\phi_F - \lambda I)\left(H_F^T H_F\right)^{-1} H_F^T \tag{36}$$

The FDF was evaluated using two gain matrices corresponding to values of 0.9 and 0.5 for the eigenvalues λ.

At each iteration of the simulation the correlations c_j' were computed for each of the four failure vectors using equation (17). The correlations were compared to the thresholds ε_j to determine if a failure had occurred. Also, the normalized correlations c_j^* were computed by dividing by the appropriate thresholds.

$$c_j^* = c_j'/\varepsilon_j \tag{37}$$

An equivalent detection criterion would be comparison of the normalized correlation c_j^* to unity. If detection occurred, the failure was identified using two different

algorithms to determine which produced better results. In the first algorithm the failure was identified ($\hat{i}$ was computed) using the correlations c_j' in equation (18); that is, $\hat{i}$ was the value of i which maximized the correlation c_j' during the run. In the second algorithm the normalized correlation c_j^* was used in place of c_j' in equation (18); that is, i^* was the value of i which maximized the normalized correlation c_j^*. Two failure magnitudes were computed using equation (19): one estimate using the correlations c_j' and the other using the normalized correlations c_j^*. Using equations (21) and (22) these computations were performed for moving windows of 1, 10, 20, and 30 samples. The time of detection, that is, the time when the correlation first crossed the threshold, was recorded.

The simulation was run at a sample rate of 20 iterations per second. Because the initial interest was in detecting and identifying catastrophic type failures, a quick reaction time was necessary. Thus, to evaluate the failure detection filter performance, only a few seconds of flight were required in a simulation run. With these constraints the aircraft could be flown open loop with no control system and still not diverge significantly from its nominal path before a failure was introduced. Therefore, to simplify the simulation the aircraft was flown open loop for all of the results discussed in this report. The aircraft was trimmed for final approach on a 3 degree glideslope.

A total of 119 simulation runs were performed to exercise the failure detection filter. The results of these runs are presented and discussed in the next section.

RESULTS

This section presents and discusses the results of the simulation runs conducted to evaluate the performance of the failure detection filter. The first results are from the aircraft simulation discussed in the preceeding section and in more detail in appendix A in which the measurements are non-linear functions of the state. A preprocessor described in appendix B is used to transform the measurements into a form suitable for use by the FDF, that is, a form in which the measurements could be approximated by linear functions of the state variables.

As discussed in the next sub-section the results led to an investigation via simulation of the filter performance using measurements which were strictly linear functions of the state (though some of these may not be physically realizable). These results together with some additional analytical results are presented and discussed in the second sub-section.

Results Using Non-Linear Measurements

Thresholds.- Using the filter gains corresponding to an eigenvalue of 0.5, three simulation runs of length 20 seconds each were made under conditions of heavy clear air turbulence ($\sigma_u = \sigma_w = 7$ ft/sec) with no failures introduced into the system. Each run was made with a different seed number for the random number generator such that each run generated a different sample function, or sequence, for the wind turbulence and for the sensor noise. From the total of these three runs the largest values ε_j computed for the correlations c_j' of the residual vector with each of the four output failure vectors using a 1-sample window of data were selected for the 1-sample threshold values. Threshold values were similarly obtained from the same runs for windows of 10, 20, and 30 samples. Three 20 second runs were made rather

than a single 60 second run because the aircraft system tended to diverge too far from the trim conditions when operating open loop for longer times. A similar set of thresholds were obtained for the filter with an eigenvalue of 0.9. These thresholds were later used in the failure detection computation and in the calculation of the normalized correlations c_j^*.

Using the 0.5 eigenvalue gains this procedure was repeated under conditions of no turbulence to obtain a set of threshold values which could be used in evaluating the effects of wind turbulence on the performance of the failure detection filter.

It was realized that this procedure would not establish a statistically reliable threshold value suitable for actual aircraft operation. However, the values thus obtained were deemed reasonable for purposes of obtaining a preliminary evaluation of the performance of the failure detection filter for aircraft control system FDI and for uncovering potential problems in using the FDF for this purpose.

Effect of eigenvalues.- Eleven simulation runs were made with each of the two filters (eigenvalues of 0.5 and 0.9) with various combinations of failures and wind turbulence levels. Detection performance is tabulated in tables III and IV and identification performance in tables VI and VII. For each filter the failures were detected in six of the eleven runs. They were correctly identified in four of the eleven runs using the maximum correlation criterion and in two runs using the maximum normalized correlation. The values for the normalized correlations c_j^* are listed in tables VIII and IX to permit comparison between the two filters and to give an indication of the "signal-to-noise" ratio, or detection margin, for the filters. From this and the other data the differences in filter performance for the two eigenvalues were deemed insignificant in this case, and the filter gains producing an eigenvalue of 0.5 were used to generate the remaining results unless otherwise indicated.

Failure detection performance.- Using the 0.5 eigenvalue filter, 28 simulation runs, including the 11 discussed in the previous paragraph, were made to evaluate the performance of the failure detection filter under various combinations of failures and turbulence standard deviations. The failures were all single point; that is, there were no multiple failures. Values for the correlation of the residuals with each of the four output failure vectors were computed at each iteration for 1-, 10-, 20-, and 30-sample data windows.

In 25 of the runs these correlation values were compared with the no turbulence threshold values to determine which failures were detected. The results, which are summarized in table V, show that 22 of the 25 failures were detected successfully. Three soft failures (the 1° elevator, the 4° throttle, and the -1° stabilizer) were not detected in zero turbulence. These failures were not detected because the thresholds values were previously determined by different sample sequences for the sensor noises, and the resulting thresholds were larger than the combination of failure and sensor noise for the sample sequence used in the failure run. These results are very optimistic in that use of the no turbulence thresholds would produce a totally unacceptable false alarm rate. However, the results are useful when compared with later results to show the degradation in performance due to wind turbulence.

The same correlation values were then compared with the thresholds obtained under conditions of heavy clear air turbulence, and the resulting detection performance is summarized in table IV. Under these conditions, that is, when the thresholds are set at the maximum correlation values obtained in heavy CAT with no failure, the failures were detected in 13 of 28 runs. Under conditions of heavy turbulence or

thunderstorm turbulence all of the failures were detected. The throttle failures were detected with some, but not all, of the data windows; other failures were detected with all of the data windows. On the other hand, under conditions of medium turbulence or zero turbulence no failures were detected. In these cases the effect of the failure alone, even with a hardover failure, was not sufficient to produce residual correlations which exceeded the thresholds.

The correlation values c_j^* for a 20-sample data window, normalized by the heavy CAT thresholds, are listed in table IX for 21 of the 28 runs. Examination of this data reveals that even though all of the failures in heavy CAT were detected, the detection margin was very small. The maximum value of c_j^* was less than 1.4, and most of the values were less than 1.1.

The instances in which failure detection occurred (not including thunderstorms) were examined to determine the time delay between failure occurrence and failure detection, that is, the time that it took after a failure for the correlation to cross the threshold. The results show that the mean detection time was 1.6 seconds and that the detection times were generally longer for the larger data windows as would be expected. A more detailed analysis of the detection times is probably not warranted since the same sample sequences were used for the turbulence and sensor noises in all of the runs, and thus additional analysis would not result in an accurate statistical picture.

Failure identification performance.- As previously discussed, two procedures were employed to perform the failure identification computations. One procedure selected the failure corresponding to the output event vector which produced the largest correlation value during the run. The other procedure selected the failure corresponding to the largest normalized correlation.

The failure identification performance is summarized in table VII. Using the heavy CAT thresholds no failures were detected in zero turbulence and medium turbulence conditions, so failure identification was not attempted in these cases. In the 13 heavy CAT and thunderstorm runs the failure was correctly identified in four runs using the maximum correlation criterion and in six runs using the maximum normalized correlation. Considering that there is an identification opportunity each time a failure is detected by a data window, there were 48 identification opportunities in these runs. Of the 48 opportunities 16 failures were correctly identified using the maximum correlation in the identification logic, and 9 were correctly identified using the maximum normalized correlation. From this data it is inconclusive as to which identification criterion produces better results, but both techniques performed poorly.

Estimates of the failure magnitude were computed for each identification opportunity, but these results were too poor to warrant further discussion.

Time histories.- Time history plots of the actual system states from the simulation and of the estimated states from the failure detection filter are shown in figures 1(a) and 1(b) for the case of no wind turbulence and the spoilers failed (stuck) at 8 degrees. Since there is no turbulence and no command input, the aircraft states are only slightly perturbed until the failure at $t = 3$ seconds. The action of the filter in tracking, or estimating, the system states can also be seen in these curves. The error in the estimate of the velocity u' is caused by the 10 ft/sec steady state wind. Plots of the 1-sample correlation of the residuals with each of the four possible output failure vectors are shown in figure 1(c). Also plotted are the correlations after normalization by the appropriate heavy CAT thresholds.

Similar plots of the correlations computed using a 20-sample data window are shown in figure 1(d). Note that none of the correlations cross the threshold, and thus no failure is detected during the 5 second run. The correlations are not calculated but are set to zero during the first 2 seconds of each run to allow the filter time to settle. The seven components of the residual vector are plotted in figure 1(e), where the effect of the failure on the residuals can be seen. Theory predicts that the residual vector should maintain a constant direction after the failure. Furthermore, after the initial transient, for a step failure the residuals should attain a steady state value equal to a constant times the output event vector, or output failure vector. Obviously neither of these conditions is true in this case.

Figure 2 contains a similar set of plots for the same 8 degree spoiler failure in heavy turbulence. Note that in this case the combined action of the turbulence and the failure have caused the correlations to exceed the threshold, and thus a failure is detected by both the 1-sample and the 20-sample windows. Note also that the 20-sample correlations are much smoother than the 1-sample correlations as expected. The residuals are quite noisy, and the effect of the failure noticed in the no turbulence run is mostly obscured in this case.

The failure detection and identification performance of the filter was not nearly as good as had been anticipated. Furthermore, the residuals did not behave in the expected manner as noted previously. In analyzing the filter in an attempt to explain these results it appeared that this behavior may be caused at least in part by the inaccuracies in the approximations made in the pre-processor in modeling the measurements as linear functions of the state variables. To better understand this effect the simulation was modified to produce a fictitious set of measurements according to the linear model, that is, measurements calculated using the H-matrix with the addition of sensor errors (noise, bias, etc.). A number of runs were made with this modification, and the results are presented in the next section.

Results Using Linear Measurements

Thresholds.- Using the simulation modified to produce linear measurements two new sets of threshold values for the filter, one set for no turbulence and one for heavy turbulence, were found employing the same procedure as before. These new thresholds were used in subsequent filter computations. The filter eigenvalues were 0.5.

Failure detection performance.- Twenty-six simulation runs were made with various failures, turbulence levels, and steady state winds to evaluate the failure detection performance of the FDF when the filter input is a set of measurements which are accurately represented by the measurement model (H-matrix) except for sensor errors. As before, the residual correlation values from these runs were compared with the appropriate no turbulence thresholds to ascertain if a failure had been detected. The results, which are summarized in table X, show that 21 out of 26 failures were detected by at least one of the detection windows. All of the failures under conditions of medium or heavy turbulence were detected, and 3 of the 8 failures in zero turbulence were detected.

The same values were compared to the heavy turbulence thresholds to evaluate the performance in a more realistic operating environment. These results, which are summarized in table XI, show that 11 out of 26 failures were detected, and five of these were spoiler failures. Only one throttle and one stabilizer failure were detected. Broken down by length of the data window, the results show that five, five, five and

eleven out of 26 failures were detected by the 30-, 20-, 10-, and 1-sample windows, respectively. These results were no better than those previously obtained with the non-linear measurements.

The normalized correlations c_j^* for a 20-sample data window are tabulated in table XIII. Significant detection margins were obtained only for the hardover spoiler failure. Other values of c_j^* were close to unity; even for the undetected failures most of the values were greater than 0.9.

Failure identification performance.- The failure identification results are summarized in table XII. In 26 identification opportunities (assuming heavy turbulence thresholds) only one failure was correctly identified using the maximum correlation value as an indicator. Only four of 26 were correctly identified using the maximum normalized correlation values. For these correct identifications the estimates of the failure magnitude were grossly inaccurate.

Time histories.- Time history plots of the 1- and 20-sample correlations and the residuals for the case of an 8 degree spoiler failure in conditions of no wind turbulence are shown in figure 3. The correlations cross the threshold between 3 and 4 seconds, and a failure is detected. If the criterion of maximum correlation is used to identify the failure, an elevator (failure 1) would be selected incorrectly. If the criterion of maximum normalized correlation is used, the 1-sample correlation would indicate an elevator failure, and the 20-sample correlation would indicate a throttle failure (failure 2). Both of these are incorrect. The residuals reach a steady state value in less than 1 second. However, there are significant residuals prior to the failure not predicted by the theory (eq. (8)).

In this regard consider the system described by the equations

$$x_{k+1} = \phi x_k + \psi u_k + \Gamma w_k \tag{38}$$

$$y_{k+1} = H x_{k+1} \tag{39}$$

where

Γ = plant disturbance (wind) input matrix

w_k = p-dimensional vector of plant disturbances (wind)

With the failure detection filter defined as before, the filter residuals for this case are described by the difference equation

$$\begin{aligned} r_{k+1} &= y_{k+1} - \hat{y}_{k+1} \\ &= H\left(x_{k+1} - \hat{x}_{k+1}\right) \\ &= H(\phi - DH)q_k + H\Gamma w_k \end{aligned} \tag{40}$$

This equation has a solution

$$r_{k+1} = H(\phi - DH)^{k+1} q_o + H \sum_{j=0}^{k} (\phi - DH)^{k-j} \Gamma w_j$$

$$= \lambda^{k+1} H q_o + \sum_{j=0}^{k} \lambda^{k-j} H \Gamma w_j \tag{41}$$

If the winds are steady state only ($w_k = w_o$), then the residual achieves a steady state value

$$r_{ss} = \frac{H \Gamma w_o}{1 - \lambda} \tag{42}$$

Comparison of the pre-failure residuals in figure 3 with the steady state residuals computed from equation (42) for a 10 ft/sec steady state wind show excellent agreement. Thus, both the theory and the simulation results show that a steady state wind will propagate through the filter like an actuator type failure. This is not to say that the steady state wind effects can never be isolated from system failures.

Plots of the residuals for an 8 degree spoiler failure with no steady state winds are shown in figure 4. In this case there are no significant residuals before the failure, but after the failure the residuals do not attain the steady state values predicted by equation (12), viz, $\alpha H f_i/(1 - \lambda)$. For an explanation of this discrepancy consider the following development.

In certain systems some of the measurements are such that actuator type failures enter directly into the measurement equation. The acceleration measurements in the B-737 system discussed in this report are in this category. Consider the following formulation of such a system.

$$x_{k+1} = \phi x_k + \psi u_k \tag{43}$$

$$y_{k+1} = H x_{k+1} + \Gamma_H B u_k \tag{44}$$

Suppose that a control surface fails in a manner that has the same effect as a command α_k in the i-th control input. Then the system is described by

$$x_{k+1} = \phi x_k + \psi u_k + \alpha_k \psi_i \tag{45}$$

$$y_{k+1} = H x_{k+1} + \Gamma_H B u_{k+1} + g_i [\alpha_{k+1} - u_{k+1}(i)] \tag{46}$$

where

$$g_i u_k(i) = \Gamma_H B \begin{bmatrix} 0 \\ \cdot \\ \cdot \\ u_k(i) \\ \cdot \\ \cdot \\ 0 \end{bmatrix} = \Gamma_H B_i u_k(i) \tag{47}$$

B_i = i-th column of B

In a manner similar to the development of equation (10) the filter residuals in this case can be shown to be described by

$$\begin{aligned} r_{k+1} &= H(\phi - DH)^{k+1} q_o + H \sum_{j=0}^{k} (\phi - DH)^{k-j} \{\alpha_j \psi_i - [\alpha_j - u_j(i)] Dg_i\} \\ &\quad + g_i [\alpha_{k+1} - u_{k+1}(i)] \\ &= H\lambda^{k+1} q_o + H \sum_{j=0}^{k} \{\lambda^{k-j} [\alpha_j (\psi_i - Dg_i) + u_j(i) Dg_i]\} \\ &\quad + g_i [\alpha_{k+1} - u_{k+1}(i)] \end{aligned} \tag{48}$$

Suppose that there are no command inputs and that the failure is a step failure of magnitude α at time zero. Then the steady state residual vector becomes

$$r_{ss} = \frac{H\alpha(\psi_i - Dg_i)}{1 - \lambda} + \alpha g_i \qquad \text{for} \quad \lambda < 1 \tag{49}$$

For the B-737 system the acceleration measurements $y_k(2)$ and $y_k(3)$ include control inputs from rows 2 and 3 of Bu_k, as in equations (A64) for $\dot{u}'$ and $\dot{\alpha}$. Examination of the B-matrix reveals that only elevator and spoiler commands, and hence failures, affect $\dot{u}'$ and $\dot{\alpha}$. Throttle and stabilizer effects enter the

measurements through the A-matrix, since thrust and stabilizer position are system state variables. Thus, the matrix Γ_H is given by

$$\Gamma_H = \begin{bmatrix} 0 & 0 & 0 & 0 & 0 & 0 \\ 0 & 1 & 0 & 0 & 0 & 0 \\ 0 & 0 & 1 & 0 & 0 & 0 \\ 0 & 0 & 0 & 0 & 0 & 0 \\ 0 & 0 & 0 & 0 & 0 & 0 \\ 0 & 0 & 0 & 0 & 0 & 0 \\ 0 & 0 & 0 & 0 & 0 & 0 \end{bmatrix} \tag{50}$$

The resulting g_2 and g_3 are zero, and

$$g_1 = \begin{bmatrix} 0 \\ 0 \\ B(3,1) \\ 0 \\ 0 \\ 0 \\ 0 \end{bmatrix} \qquad g_4 = \begin{bmatrix} 0 \\ B(2,4) \\ B(3,4) \\ 0 \\ 0 \\ 0 \\ 0 \end{bmatrix} \tag{51}$$

Comparison of the residuals predicted by equation (49) for an 8 degree spoiler failure with the post-failure steady state residuals in figure 4 show very good agreement.

Equations (48) show that for systems with measurements of this type the filter residuals are not constrained to a constant direction Hf_i as previously discussed but are constrained to the plane defined by the vectors $H\psi_i$ and HDg_i. This characteristic increases the complexity of the failure identification process.

In figure 5 are plots of the residuals for an 8 degree spoiler failure with no winds where the failure occurs as a ramp over 1.5 seconds rather than a step as in previous cases. Here the residual vector appears to maintain a fairly constant direction during the failure as expected from the theory.

In table XIV are the steady state correlations $c'(j,k)$ for hardover failures, that is, the correlations of the output event vectors, or output failure vectors, with the steady state residuals for hardover failures, where the correlations were computed according to the equation

$$c'(j,k) = \langle Hf_j, r_{ss_k} \rangle \frac{(1 - \lambda)}{|Hf_j|} \tag{52}$$

Values of j and k from 1 to 4 correspond to 10, 40, -6, and 8 degree failures of the elevator, throttle, stabilizer, and spoiler, respectively. Values of 5 and 6 correspond to 10 ft/sec and 1 ft/sec steady state winds in the x- and z-directions, respectively. The winds were treated as failures as discussed in equations (38) through (42). The steady state residuals were computed using equation (49) for k equal to 1 through 4 and using equation (42) for k equal to 5 and 6. Note that in these results the actual failures 1 through 6 correspond to columns 1 through 6 and the assumed failures 1 through 6, that is, the output event vectors used to correlate with the residuals, correspond to rows 1 through 6.

The results show that using the maximum correlation value as the criterion for identification an elevator failure (failure 1) would be incorrectly identified as a stabilizer failure (failure 3). Also, a spoiler failure would be incorrectly identified as an elevator failure. This behavior is the result of the elevator and spoiler failures directly affecting the measurement equation and hence the residuals via the acceleration measurements.

Model mis-match.- To assess the effects of inaccuracies in the filter model on FDF performance three runs were made using a different aircraft model in the filter than in the simulation. The model used in the filter was the landing configuration model previously used in the other runs, while the aircraft simulation used a model of the takeoff configuration. The three runs were similar to the runs used to determine the thresholds; that is, each run lasted 20 seconds in heavy turbulence with no failure.

False alarms were declared in two of the three runs. In other words, the filter model errors caused the correlations to exceed the thresholds and to falsely declare a failure in two of the runs. Further investigation is required to determine the amount of increase in the threshold levels needed as a function of the degree of model error to prevent a false alarm problem due to mis-match. It is reasonable to expect that different models may be required for operation in the different flight regimes.

CONCLUSIONS

The application of the failure detection filter to the detection and identification of control element failures in transport aircraft has been evaluated using a linear digital simulation of a B-737 airplane. With the thresholds set at a level determined by heavy clear air turbulence approximately one half of the failures in the elevator, throttle, stabilizer, and spoiler were successfully detected. However, in heavy CAT and in thunderstorms all of the failures were detected, while in lesser turbulence none were detected.

The primary reason for the missed detections at the lower turbulence levels was the necessity to set the thresholds sufficiently high to avoid false alarms caused by wind turbulence. With the thresholds set at a level determined by the sensor noise with zero turbulence 23 out of 25 failures were detected. Thus, with the FDF and correlation processor used in this evaluation the detection performance was affected as much by the turbulence as by the failure.

The measurements used as inputs to the FDF were non-linear functions of the aircraft states. Replacing these with measurements which were linear functions of the states as modeled by the H-matrix did not result in significant improvement in

filter performance. Further degradation in performance was caused by mis-match, or inaccuracies, in the aircraft model used in the FDF.

With some measurements, such as the acceleration measurements in this system, some actuator type failures feed directly into the measurement equation with the result that the filter residuals from these failures cannot be confined to a constant direction in measurement space. Also, with the state space formulation used in this evaluation a steady state wind affects the filter residuals in the same way as does an actuator type failure.

From the results of the simulation runs, it is concluded that false alarms/ missed detections due to wind turbulence are a significant problem which must be overcome before the failure detection filter and correlation processor can be used to detect and identify control element failures in a transport aircraft.

APPENDIX A

SIMULATION DESCRIPTION

The Aircraft

The system used to evaluate the failure detection filter was a discrete, linear, small perturbation simulation of the longitudinal channel of a B-737 aircraft similar to the simulation described by Halyo in reference 20. Much of the development in this appendix follows that by Halyo. The discrete system was derived from a continuous time system described by the following state equations:

$$\dot{x}(t) = Ax(t) + Bu(t) + Dw(t) \tag{A1}$$

where the state vector $x(t)$ is a 6-component vector defined as

$$x(t) = \begin{bmatrix} \theta \\ u' \\ \alpha \\ q \\ \delta T \\ \delta S \end{bmatrix} \tag{A2}$$

and where the perturbed states are

θ = pitch

u' = normalized x-velocity

α = angle-of-attack

q = pitch rate

δT = thrust

δS = stabilizer deflection

The thrust and stabilizer states were included to account for the engine spool up/spool down time and for the time constant in the stabilizer actuator. The command vector $u(t)$ is defined by

$$u(t) = \begin{bmatrix} \delta e \\ \delta th \\ \delta st \\ \delta sp \end{bmatrix} \tag{A3}$$

where

δe = elevator command (= elevator position)

δth = throttle command

δst = stabilizer command

δsp = spoiler command (= spoiler position)

The wind vector is defined by

$$w(t) = \begin{bmatrix} u'_w \\ \alpha_w \\ q_w \end{bmatrix} \tag{A4}$$

where the wind components are

u'_w = normalized wind velocity in the negative x-direction

α_w = part of the angle-of-attack due to winds

q_w = rotation of the atmosphere about the y-axis

Unless otherwise specified, the quantities are defined and the equations are written in the aircraft's stability axes.

Values for the system matrices were obtained using a computer program (TCVOPL) which computes the aerodynamic coefficients for aircraft trim conditions specified by the program user. Exceptions to this procedure are the coefficients for the thrust and stabilizer states. The engine thrust is modeled as

$$\begin{aligned} \dot{\delta T} &= A_{55}\delta T + B_{52}\delta th \\ &= -0.5\ \delta T + 0.298\ \delta th \end{aligned} \tag{A5}$$

The value 0.5 was approximated from engine data for the B-737.

The response of the stabilizer on the B-737 is very slow. In order to have another control surface for restructurable controls, the time constant of the stabilizer was artificially shortened to make the surface useful. The stabilizer dynamics were assumed to be

$$\begin{aligned} \dot{\delta S} &= A_{66}\delta S + B_{63}\delta st \\ &= -0.667\ \delta S + 0.667\ \delta st \end{aligned} \tag{A6}$$

The Winds

The wind effects on the aircraft are simulated by adding them to the other aerodynamic forces acting on the aircraft. As noted in equation (A4) the wind is composed of x-velocity, angle-of-attack, and pitch rate components, and they include both steady state winds and wind gusts, or turbulence.

The gust components are modeled using the familiar Dryden spectra (ref. 19), which are defined by the following:

$$S_u(\Omega) = \frac{2\sigma_u^2 L_u}{1 + (L_u\Omega)^2} \tag{A7}$$

$$S_\alpha(\Omega) = \frac{\sigma_w^2 L_w}{V_a^2} \cdot \frac{1 + 3(L_w\Omega)^2}{\left[1 + (L_w\Omega)^2\right]^2} \tag{A8}$$

$$S_q(\Omega) = \frac{\Omega^2 V_a^2}{1 + \left(\frac{4b\Omega}{\pi}\right)^2} \cdot S_\alpha(\Omega) \tag{A9}$$

$$S_{q\alpha}(\Omega) = \frac{j\Omega}{1 + \frac{j4b\Omega}{\pi}} S_\alpha(\Omega) \tag{A10}$$

In equations (A7) through (A10) σ_u^2 and σ_w^2 are the variances of the gust velocities in the x- and z-axes, respectively, L_u and L_w are the turbulence scales in these axes, b is the aircraft wingspan, V_a is the aircraft airspeed, and Ω is the spatial frequency of the turbulence, which is related to the temporal frequency ω by

$$\omega = \Omega V_a \tag{A11}$$

In order to use these spectra in the simulation, which generates random gusts as a function of time, the spectra must be converted from functions of spatial frequency to functions of temporal frequency using the relationship

$$S(\omega) = \frac{1}{V_a} S(\omega/V_a) \tag{A12}$$

Angle-of-attack component.- Upon conversion to a function of ω the spectral density of α_g becomes

$$S_\alpha(\omega) = \frac{\sigma_w^2 L_w}{V_a^3} \cdot \frac{1 + 3(L_w/V_a)^2\omega^2}{\left[1 + (L_w/V_a)^2\omega^2\right]^2} \tag{A13}$$

which can be factored into

$$S_\alpha(\omega) = \frac{\sigma_w^2 L_w}{V_a^3} \cdot \frac{1 + j\sqrt{3}\,(L_w/V_a)\omega}{\left[1 + j(L_w/V_a)\omega\right]^2} \cdot \frac{1 - j\sqrt{3}\,(L_w/V_a)\omega}{\left[1 - j(L_w/V_a)\omega\right]^2} \tag{A14}$$

Define a transfer function $G_\alpha(s)$ using the realizable part of the spectrum in (A14).

$$G_\alpha(s) = \frac{1 + \sqrt{3}\,(L_w/V_a)s}{\left[1 + (L_w/V_a)s\right]^2} \tag{A15}$$

$$= \frac{1 + \sqrt{3}\,(L_w/V_a)s}{1 + 2(L_w/V_a)s + (L_w/V_a)^2 s^2}$$

A filter with this transfer function driven by white noise with a density of $\sigma_w^2 L_w/V_a^3$ will produce random gusts with the spectral density specified by equation (A13) and with variance σ_w^2/V_a^2.

Let us now turn our attention to obtaining a set of state equations which describe the filter specified by equations (A15). First convert the transfer function to an equivalent scalar differential equation.

$$\left(\frac{L_w}{V_a}\right)^2 \ddot{\alpha}_g + \frac{2L_w}{V_a}\dot{\alpha}_g + \alpha_g = \frac{\sqrt{3}\,L_w}{V_a}\dot{\xi} + \xi$$

or

$$\ddot{\alpha}_g + \frac{2V_a}{L_w}\dot{\alpha}_g + \left(\frac{V_a}{L_w}\right)^2 \alpha_g = \frac{\sqrt{3}\,V_a}{L_w}\dot{\xi} + \left(\frac{V_a}{L_w}\right)^2 \xi \tag{A16}$$

Now let $y = -\alpha_g$ and $\xi_1 = -\xi$ in equation (A16), and let

$$W_1 = y = -\alpha_g$$

$$\dot{W}_1 = W_2 + c_1 \xi_1 \tag{A17}$$

$$\dot{W}_2 = -2(V_a/L_w)W_2 - (V_a/L_w)^2 W_1 + c_2 \xi_1$$

From equations (A17) find expressions for $\dot{y}$ and $\ddot{y}$.

$$\dot{y} = W_2 + c_1 \xi_1$$

$$\ddot{y} = -2(V_a/L_w)W_2 - (V_a/L_w)^2 W_1 + c_2 \xi_1 + c_1 \dot{\xi}_1 \tag{A18}$$

Substitute these in equation (A16), and solve for c_1 and c_2.

$$c_1 = \sqrt{3}\ (V_a/L_w)$$

$$c_2 = (1 - \sqrt{12})(V_a/L_w)^2 \tag{A19}$$

Pitch component.- Upon conversion to a function of ω the power spectral density of the pitch gusts becomes

$$S_q(\omega) = \frac{\omega^2}{1 + (4b/\pi V_a)^2 \omega^2} S_\alpha(\omega)$$

$$= \frac{j\omega}{1 + j(4b/\pi V_a)\omega} G_\alpha(j\omega) \cdot \frac{-j\omega}{1 - j(4b/\pi V_a)\omega} G_\alpha(-j\omega) \tag{A20}$$

The wind gusts in pitch can be simulated by passing angle-of-attack gusts, that is the output of the filter $G_\alpha(s)$, through a filter with a transfer function $G_q(s)$ defined by

$$G_q(s) = \frac{s}{1 + (4b/\pi V_a)s} \tag{A21}$$

To obtain a state variable representation of the filter, first find the scalar differential equation equivalent of the transfer function $G_q(s)$.

$$\frac{4b}{\pi V_a}\dot{q}_g + q_g = \dot{\alpha}_g = -\dot{w}_1 \tag{A22}$$

Let

$$q_g = -\frac{\pi V_a}{4b} w_1 + \frac{\pi V_a}{4b} w_3 \tag{A23}$$

Then

$$-\dot{w}_1 + \dot{w}_3 - \frac{\pi V_a}{4b} w_1 + \frac{\pi V_a}{4b} w_3 = -\dot{w}_1 \tag{A24}$$

Therefore

$$\dot{w}_3 = \frac{\pi V_a}{4b} w_1 - \frac{\pi V_a}{4b} w_3 \tag{A25}$$

X-axis component.- Upon conversion to a function of ω the power spectral for the gusts along the x-axis becomes

$$S_u(\omega) = \frac{2L_u\sigma_u^2}{V_a^3} \cdot \frac{1}{1 + (L_u/V_a)^2\omega^2} \tag{A26}$$

$$= \frac{2L_u\sigma_u^2}{V_a^3} \cdot \frac{1}{1 + j(L_u/V_a)\omega} \cdot \frac{1}{1 - j(L_u/V_a)\omega}$$

The x-axis gusts can be obtained by passing white noise with density $2L_u\sigma_u^2/V_a^3$ through a filter with transfer function $G_u(s)$ defined by

$$G_u(s) = \frac{1}{1 + (L_u/V_a)s} \tag{A27}$$

The corresponding scalar differential equation is

$$\frac{L_u}{V_a}\dot{u}'_g + u'_g = \xi_2 \tag{A28}$$

or in terms of state variables

$$\begin{aligned} W_4 &= u'_g \\ \dot{W}_4 &= -\frac{V_a}{L_u} W_4 + \frac{V_a}{L_u}\xi_2 \end{aligned} \tag{A29}$$

Steady state winds.- The steady state winds have an x-axis component and an angle-of-attack component each of which is simulated as the output of a first order differential equation driven by white noise with a very small variance. This allows the winds to vary slightly during a run. The desired steady state wind velocities are used as the initial conditions. Mathematically the winds are described as follows:

$$\begin{aligned} \dot{u}'_s(t) &= \xi_3; \qquad u'_s(0) = u_s(0)/U_o \\ \dot{\alpha}_s(t) &= \xi_4; \qquad \alpha_s(0) = w_s(0)/U_o \end{aligned} \tag{A30}$$

Wind state equations.- Equations (A17), (A25), (A29), and (A30) can be combined to describe the total winds as follows:

$$\dot{W} = A_W W + B_W \xi \tag{A31}$$

where

$$W = \begin{bmatrix} W_1 \\ W_2 \\ W_3 \\ W_4 \\ W_5 \\ W_6 \end{bmatrix}$$

$$A_W = \begin{bmatrix} 0 & 1 & 0 & 0 & 0 & 0 \\ -\left(V_a^2/L_w^2\right) & -(2V_a/L_w) & 0 & 0 & 0 & 0 \\ (\pi V_a/4_b) & 0 & -(\pi V_a/4_b) & 0 & 0 & 0 \\ 0 & 0 & 0 & -(V_a/L_u) & 0 & 0 \\ 0 & 0 & 0 & 0 & 0 & 0 \\ 0 & 0 & 0 & 0 & 0 & 0 \end{bmatrix} \tag{A32}$$

$$\xi = \begin{bmatrix} \xi_1 \\ \xi_2 \\ \xi_3 \\ \xi_4 \end{bmatrix} \tag{A33}$$

$$B_W = \begin{bmatrix} \left(\sqrt{3}\ V_a/L_w\right) & 0 & 0 & 0 \\ \left(1 - \sqrt{12}\right) \cdot (V_a/L_w) & 0 & 0 & 0 \\ 0 & 0 & 0 & 0 \\ 0 & (V_a/L_u) & 0 & 0 \\ 0 & 0 & 1 & 0 \\ 0 & 0 & 0 & 1 \end{bmatrix} \tag{A34}$$

The covariance matrix of the Gaussian vector ξ is

$$F = E\{\xi\xi^T\}$$

$$F = \begin{bmatrix} (\sigma_w^2 L_w/V_a^3) & 0 & 0 & 0 \\ 0 & (2L_u\sigma_u^2/V_a^3) & 0 & 0 \\ 0 & 0 & 1/V_a^3 & 0 \\ 0 & 0 & 0 & 1/V_a^3 \end{bmatrix} \tag{A35}$$

In the foregoing formulation the wind gusts W_1 through W_4 were written in aircraft body axes, and the steady state winds W_5 and W_6 were written in earth axes. They must be transformed into stability axes. Furthermore, the gust and steady state components must be added, and W_1 and W_3 must be combined according to equation (A2) in order to obtain proper wind forces acting on the aircraft. This can all be accomplished with the transformation C_W as follows:

$$w = C_W W \tag{A36}$$

where

$$w = \begin{bmatrix} w_1 \\ w_2 \\ w_3 \end{bmatrix} = \begin{bmatrix} u'_w \\ \alpha_w \\ q_w \end{bmatrix} = \begin{bmatrix} u'_g + u'_s \\ \alpha_g + \alpha_s \\ q_g \end{bmatrix} \tag{A37}$$

and

$$C_W = \begin{bmatrix} -\sin\alpha_o & 0 & 0 & -\cos\alpha_o & -\cos(\theta_o - \alpha_o + \theta) & \sin(\theta_o - \alpha_o + \theta) \\ -\cos\alpha_o & 0 & 0 & \sin\alpha_o & -\sin(\theta_o - \alpha_o + \theta) & -\cos(\theta_o - \alpha_o + \theta) \\ -(\pi V_a/4b) & 0 & (\pi V_a/4b) & 0 & 0 & 0 \end{bmatrix} \tag{A38}$$

Discrete State Equations

The state equations for the aircraft and winds have been written as functions of continuous time t. These equations need to be coverted to functions of discrete time t_k for use in a digital computer simulation. Such a discretization has been discussed by Halyo (ref. 20).

Consider the aircraft continuous time state equation (A1). If the state is known at time t_k, the state at time $t_{k+1} = t_k + T$ can be found by integration over the interval t_k to t_{k+1}. The result is shown in many texts (e.g., ref. 21) to be

$$x(t_{k+1}) = \phi(t_{k+1},t_k)x(t_k) + \int_{t_k}^{t_{k+1}} \phi(t_{k+1},\tau)Bu(\tau)\, d\tau$$

$$+ \int_{t_k}^{t_{k+1}} \phi(t_{k+1},\tau)Dw(\tau)\, d\tau \qquad \text{(A39)}$$

where

$$\phi(t,\tau) = e^{A(t-\tau)}$$

To simplify the notation, let $x(t_k)$ be denoted by x_k, and assume that the command $u(t)$ is constant over the integral $t_k \leq t < t_{k+1}$. Then

$$x_{k+1} = \phi(k+1,k)x_k + \int_{t_k}^{t_{k+1}} \phi(t_{k+1},\tau)\, d\tau\, Bu_k$$

$$+ \int_{t_k}^{t_{k+1}} \phi(t_{k+1},\tau)Dw(\tau)\, d\tau \qquad \text{(A40)}$$

The integral $\int_{t_k}^{t_{k+1}} \phi(t_{k+1},\tau)\, d\tau$ can be expressed as

$$\int_{t_k}^{t_{k+1}} e^{A(t_{k+1}-\tau)}\, d\tau\, B = e^{At_{k+1}} \int_{t_k}^{t_{k+1}} e^{-A\tau}\, d\tau\, B \qquad \text{(A41)}$$

If A has an inverse A^{-1}, then

$$\psi = \int_{t_k}^{t_{k+1}} e^{A(t_{k+1}-\tau)}\, d\tau\, B = e^{At_{k+1}} \int_{t_k}^{t_{k+1}} e^{-At} A^{-1}\, d(A\tau)B$$

$$= e^{At_{k+1}}\left[-e^{-At_{k+1}} + e^{-At_k}\right]A^{-1}B \qquad \text{(A42)}$$

$$= [\phi(k+1,k) - I]A^{-1}B$$

The aircraft state equation now becomes

$$x_{k+1} = \phi x_k + \psi u_k + \int_{t_k}^{t_{k+1}} \phi(t_{k+1},\tau)Dw(\tau)\, d\tau \qquad \text{(A43)}$$

To evaluate the integral involving the wind $w(\tau)$, we first convert the continuous time wind state equation (A31) to discrete time.

$$\dot{W} = A_W W + B_W \xi \qquad \text{(A31)}$$

Upon integration this becomes

$$W_{k+1} = \phi_W W_k + \xi_k \qquad \text{(A44)}$$

where ϕ_W is the state transition matrix for the wind system.

$$\phi_W = \phi_W(k+1,\, k)$$

$$= e^{A_W(t_{k+1}-t_k)} \qquad \text{(A45)}$$

and

$$\xi_k = \int_{t_k}^{t_{k+1}} \phi_W(t_{k+1},\tau)B_W\xi(\tau)\,d\tau$$

$$= \int_0^T \phi_W(T,\tau)B_W\xi(t_k+\tau)\,d\tau \qquad \text{(A46)}$$

Halyo (ref. 20) has shown that ξ_k is a Gaussian white noise vector sequence with covariance R_ξ.

$$R_\xi(k,j) = E\{\xi_k\xi_j^T\}$$

$$= E\left\{\int_0^T \phi_W(T,\tau)B_W\xi(t_k+\tau)\,d\tau \cdot \int_0^T \xi^T(t_j+s)B_W^T\phi_W^T(T,s)\,ds\right\} \qquad \text{(A47)}$$

$$= \int_0^T\int_0^T \phi_W(T,\tau)B_W E\{\xi(t_k+\tau)\xi^T(t_j+s) \cdot B_W^T\phi_W^T(T,s)\,d\tau\,ds$$

Since $\xi(t)$ is a white noise process, and since the intervals (t_k,t_k+T) and (t_j,t_j+T) do not overlap for $j\neq k$,

$$E\{\xi(t_k+\tau)\xi^T(t_j+s)\} = \begin{cases} 0 & j\neq k \\ F\delta(\tau-s) & j=k \end{cases} \qquad \text{(A48)}$$

Therefore,

$$R_\xi(k,j) = R_\xi\delta_{jk} \qquad \text{(A49)}$$

$$R_\xi = \int_0^T \phi_W(T,s)B_W F B_W^T\phi_W(T,s)\,ds \qquad \text{(A50)}$$

The matrix C_W, which transforms the continuous time wind variables W into the variables w for use as the plant noise in the aircraft state equations, is still valid for the discrete case. Thus

$$w_k = C_W W_k \tag{A51}$$

We now return to the evaluation of the integral in equation (A43) involving the wind $w(\tau)$. A change of variables produces

$$\int_{t_k}^{t_{k+1}} \phi(t_{k+1},\tau) Dw(\tau)\, d\tau = \int_0^T \phi(T,s) Dw(t_k + s)\, ds \tag{A52}$$

After substitution of equation (A36), integration of equation (A44) from 0 to T, and substitution of equation (A46), the integral becomes

$$\int_0^T \phi(T,s) Dw(t_k + s)\, ds = \int_0^T \phi(T,s) DC_W \phi_W(s,0)\, ds\, W_k + \int_0^T \phi(T,s) DC_W \int_0^s \phi_W(s,\tau) B_W \xi(t_k + \tau)\, d\tau\, ds \tag{A53}$$

The aircraft state equation can now be written as

$$x_{k+1} = \phi x_k + \psi u_k + \Gamma_W W_k + \eta_k \tag{A54}$$

where

$$\Gamma_W = \int_0^T \phi(T,s) DC_W \phi_W(s,0)\, ds \tag{A55}$$

and

$$\eta_k = \int_0^T \phi(T,s) DC_W \int_0^s \phi_W(s,\tau) B_W \xi(t_k + \tau)\, d\tau\, ds \tag{A56}$$

The sequence η_k is a Gaussian white noise vector sequence with covariance R_η.

$$R_\eta(k,j) = E\{\eta_k \eta_j^T\}$$

$$= \int_0^T \int_\tau^T \phi(T,s) DC_W \phi_W(s,\tau)\, ds\; B_W \xi(t_k + \tau)\, d\tau$$

$$\cdot \int_0^T \xi(t_j + y) B_W^T \int_y^T \phi_W^T(x,y) C_W^T \phi^T(T,x)\, dx\, dy \qquad \text{(A57)}$$

$$= \int_0^T \int_0^T \int_\tau^T \phi(T,s) DC_W \phi_W(s,\tau)\, ds\; B_W E\{\xi(t_k + \tau)\xi^T(t_j + y)\}$$

$$\cdot B_W^T \int_y^T \phi_W^T(x,y) C_W^T D^T \phi^T(T,x)\, dx\, dy\, d\tau$$

As we noted previously in equation (A48),

$$E\{\xi(t_k + \tau)\xi^T(t_j + y)\} = \begin{cases} 0 & j \neq k \\ F\delta(\tau - y) & j = k \end{cases} \qquad \text{(A58)}$$

Therefore

$$R_\eta(j,k) = R_\eta \delta_{jk} \qquad \text{(A59)}$$

$$R_\eta = \int_0^T \left[\int_\tau^T \phi(T,s) DC_W \phi_W(s,\tau)\, ds \right] B_W F B_W^T$$

$$\left[\int_\tau^T \phi_W^T(x,\tau) C_W^T D^T \phi^T(T,x)\, dx \right] d\tau \qquad \text{(A60)}$$

This completes the discretization of the state equations necessary to simulate the aircraft and winds.

Measurements

Thus far we have described the simulation of the aircraft dynamics and of the winds acting on the aircraft. For the purposes of the work discussed in this report the simulation needs one additional element - simulation of the measurements, or aircraft sensor outputs.

The measurements of interest are pitch attitude from a pitch gyro, x- and z-accelerations from body mounted accelerometers, pitch rate from a pitch rate gyro, airspeed and altitude rate from the air data computer, and angle-of-attack from an angle-of-attack vane. A reasonably accurate simulation requires computation of the true value of the quantity being measured and then the addition of appropriate errors. For each measurement these errors include some, but not necessarily all, of the following: bias, white noise, scale factor, and alignment. The true values and errors are combined at each sample time t_k to form a measurement vector z_k.

$$z_k = \begin{bmatrix} z_k(1) \\ z_k(2) \\ \vdots \\ z_k(7) \end{bmatrix} \tag{A61}$$

Pitch.- The pitch measurement includes additive noise and bias errors.

$$z_k(1) = \theta + v_k(1) + b(1) \tag{A62}$$

where

θ = pitch = $x_k(1)$

$b(1) = 0.23°$

$v_k(1)$ = zero mean white Gaussian noise

$E\{v_k^2(1)\} = (0.23°)^2$

Accelerations.- The x- and z-axis acceleration measurements include noise, bias, scale factor, and misalignment errors. The first step in obtaining a simulated measurement is to compute the true value of the acceleration in stability coordinates, A_{x_s} and A_{z_s}, from the equations of motion.

$$A_{x_s} = U_o\dot{u}' + qU_o \tan \alpha + g \sin(\theta_o + \theta - \alpha_o)$$

$$A_{z_s} = U_o[\dot{u}' \tan \alpha + (1 + u')\dot{\alpha}/\cos^2 \alpha] - qU_o - g \cos(\theta_o + \theta - \alpha_o) \quad \text{(A63)}$$

where

g = acceleration due to gravity

U_o = trim inertial velocity along x

θ_o = trim pitch attitude

α_o = trim angle-of-attack

θ = perturbed pitch = $x_k(1)$

u' = perturbed inertial velocity along x = $x_k(2)$

α = perturbed inertial angle of attack = $x_k(3)$

q = perturbed pitch rate = $x_k(4)$

At any time t_k values of x_k are known from the aircraft state equation. The quantities $\dot{u}'$ and $\dot{\alpha}$ are calculated using the coefficients from the continuous time state equation.

$$\left.\begin{aligned} \dot{u}' &= \varepsilon_2^T[Ax_k + Bu_k + Dw_k] \\ \dot{\alpha} &= \varepsilon_3^T[Ax_k + Bu_k + Dw_k] \end{aligned}\right\} \quad \text{(A64)}$$

where

$$\varepsilon_2^T = [0\ 1\ 0\ 0\ 0\ 0]$$

$$\varepsilon_3^T = [0\ 0\ 1\ 0\ 0\ 0]$$

These stability axis accelerations are transformed into body axis accelerations, and the effects of accelerometer misalignment are added as follows:

$$\left.\begin{aligned} A_{x_b} &= A_{x_s} \cos(\alpha_o + a) - A_{z_s} \sin(\alpha_o + a) \\ A_{z_b} &= A_{x_s} \sin(\alpha_o + a) + A_{z_s} \cos(\alpha_o + a) \end{aligned}\right\} \quad \text{(A65)}$$

where

a = accelerometer alignment error = 0.2°

Noise, bias, and scale factor errors are added to obtain the acceleration measurements.

$$\left.\begin{aligned} z_k(2) &= \left[A_{x_b} + v_k(2) + b(2)\right] \cdot (1 + s) \\ z_k(3) &= \left[A_{z_b} + v_k(3) + b(3)\right] \cdot (1 + s) \end{aligned}\right\} \quad \text{(A66)}$$

where

s = scale factor error = .0025

$b(2) = b(3)$ = bias = 0.32 ft/sec^2

$v_k(2), v_k(3)$ = zero mean Gaussian noise

$E\{v_k^2(2)\} = E\{v_k^2(3)\} = (0.32 \text{ ft/sec}^2)^2$

Pitch rate.- The pitch rate measurement includes only a noise error.

$$z_k(4) = q + v_k(4) \quad \text{(A67)}$$

where

q = pitch rate = $x_k(4)$

$v_k(4)$ = zero mean Gaussian noise

$E\{v_k^2(4)\} = (.02 \text{ deg/sec})^2$

Air speed.- The air speed measurement includes a multiplicative noise error and a bias.

$$z_k(5) = V_a\left[1 + v_k(5)\right] + b(5) \tag{A68}$$

where

$V_a = U_o(1 + u' + u'_w)/\cos(\alpha + \alpha_w)$

u' = normalized inertial velocity along $x = x_k(2)$

u'_w = normalized wind velocity along $x = w_k(1)$

α = angle-of-attack due to inertial velocity along $z = x_k(3)$

α_w = angle-of-attack due to wind velocity along $z = w_k(2)$

$b(5) = 3$ kts

$v_k(5)$ = zero mean Gaussian noise

$E\{v_k^2(5)\} = (0.02)^2$

Altitutde rate.- The altitude rate measurement includes only a noise error.

$$z_k(6) = \dot{h} + v_k(6) \tag{A69}$$

where

$\dot{h} = U_o(1 + u')\left[\sin(\theta_o + \theta - \alpha_o) - \tan\alpha\cos(\theta_o + \theta - \alpha_o)\right]$

$v_k(6)$ = zero mean Gaussian noise

$E\{v_k^2(6)\} = (5 \text{ ft/sec})^2$

Angle-of-attack.- The angle-of-attack measurement includes bias and additive noise errors.

$$z_k(7) = \alpha + \alpha_w + v_k(7) + b(7) \tag{A70}$$

where α and α_w were previously defined, and $v_k(7)$ is zero mean Gaussian noise. The bias $b(7)$ and noise error variance were estimated to be $0.25°$ and $(0.4°)^2$, respectively.

The measurement errors are summarized in table A1.

TABLE A1.- MEASUREMENT ERRORS

Measurement	Error type			
	Noise standard deviation	Bias	Scale factor	Alignment
Pitch	0.23°	0.23°	-	-
Acceleration	0.32 $\frac{ft}{sec^2}$	0.32 $\frac{ft}{sec^2}$	0.0025	0.2°
Pitch rate	0.02 $\frac{deg}{sec}$	-	-	-
Air speed	0.02*	3.0 kts	-	-
Altitude rate	5 $\frac{ft}{sec}$	-	-	-
Angle-of-attack	0.4°	0.25°	-	-

*multiplicative

Implementation

Implementation of these equations into the simulation requires evaluation of the integrals in the expressions for Γ_w, R_ξ, and R_η in equations (A55), (A50), and (A60), respectively. The integrals in equations (A55) and (A50) and the inner integrals in equation (A60) were evaluated using a Langley software library subroutine GLEGEN, which performs numerical integration using a Gauss-Legendre formula. The outer integral in equation (A60) was evaluated using the library subroutine SIMP, which performs numerical integration using Simpson's formula. In all cases, the aircraft transition matrix was evaluated using the library subroutine CONEXP, which computes the matrix exponential.

Random sequences.- The random sequences ξ_k and η_k have correlation matrices R_ξ and R_η defined by equations (A50) and (A60), respectively. In general, these matrices are not diagonal, and thus the components $\xi_k(1)$, $\xi_k(2)$, ..., $\xi_k(6)$ of the vector ξ_k are not independent as they were with the vector $\xi(t)$ in the continuous time case. This is also true of the components $\eta_k(1)$, $\eta_k(2)$, ..., $\eta_k(6)$ of η_k.

At time t_k the simulation generates a vector ξ_k of 6 random numbers with covariance matrix R_ξ using the following technique. Let x be a vector of zero

mean, independent, Gaussian random variables with unity variance. Then the correlation matrix R_x is

$$R_x = E\{xx^T\}$$
$$= I \tag{A71}$$

Let y be the vector of desired zero mean random variables $y_1, y_2, \ldots, y_N$ with the covariance matrix R_y. Now let the desired random vector y be given by

$$y = Gx \tag{A72}$$

where the transformation G is defined to produce the desired covariance of y, that is

$$E\{yy^T\} = E\{Gxx^TG^T\}$$
$$= GE\{xx^T\}G^T \tag{A73}$$
$$= GG^T$$

Therefore

$$GG^T = R_y \tag{A74}$$

If G is assumed to be triangular, one solution (of many) to equation (A74) is given by the following:

$$y_1 = g_{11}x_1$$
$$y_2 = g_{21}x_1 + g_{22}x_2$$
$$\vdots \tag{A75}$$
$$y_N = g_{N1}x_1 + g_{N2}x_2 + \cdots + g_{NN}x_N$$

Then

$$E\{y_1^2\} = R_{11} = g_{11}^2$$

$$E\{y_2 y_1\} = R_{21} = g_{11} g_{21}$$

$$E\{y_2^2\} = R_{22} = g_{21}^2 + g_{22}^2 \qquad \text{(A76)}$$

$$\vdots$$

This system of equations can be solved for the elements g_{ij} to give

$$g_{11} = \sqrt{R_{11}}$$

$$g_{j1} = R_{j1}/g_{11} \qquad 2 \leq j \leq N$$

$$g_{ji} = \left(R_{ji} - \sum_{m=1}^{i-1} g_{jm} g_{im}\right) \Big/ g_{ii} \qquad 1 < i < j \qquad \text{(A77)}$$

$$g_{jj} = \left\{R_{jj} - \sum_{m=1}^{j-1} g_{jm}^2\right\}^{1/2} \qquad 2 \leq j \leq N$$

The same technique is used to generate the vector η_k of random numbers with covariance R_η.

Failures.- Failures in the control elements were simulated as steps or ramps in the state variables according to

$$x_{k+1} = \phi x_k + \psi u_k + \Gamma_w w_k + \eta_k + \alpha_k f_i \delta_{k+1,\theta} \qquad \text{(A78)}$$

where

$f_i = \psi_i$

= i-th column of the control transition matrix.

and α_k is chosen to be a step or ramp.

Because the acceleration measurements $z_k(2)$ and $z_k(3)$ contain terms which include the continuous time control input matrix B as in equations (A64) through (A66), any failure affecting these terms must be accounted for in the simulated measurements. For the four failures simulated, only the elevator and spoiler failures affected the B-matrix and thus introduced failure effects directly into the measurement equation via the expressions for $\dot{u}'$ and $\dot{\alpha}$. For a stuck actuator these effects were simulated by adding terms to equation (A64) as follows:

$$\dot{u}' = \varepsilon_2^T \{Ax_k + Bu_k + Dw_k + B_i[\alpha_k - u_k(i)]\}$$

$$\dot{\alpha} = \varepsilon_3^T \{Ax_k + Bu_k + Dw_k + B_i[\alpha_k - u_k(i)]\} \qquad \text{(A79)}$$

where

B_i = i-th column of B

$u_k(i)$ = i-th component of the control vector u_k

The term $B_i \alpha_k$ accounts for the failure and the term $B_i u_k(i)$ accounts for the loss of that control input.

APPENDIX B

THE PRE-PROCESSOR

The failure detection filter requires input measurements that can be expressed as linear functions of the state variables as in equation (35). As noted in the text, the actual measurements z_k do not meet this requirement. A pre-processor was used to obtain from the measurements a set of pseudo-measurements y_k which could be approximated by a linear model. This pre-processor is described in the following paragraphs.

Not only are the actual measurements non-linear functions of the state variables in some cases, but some measurements are functions of the winds, which are not included in the filter state vector. Therefore, one of the approximations that must be made in obtaining a linear model of the measurements is to neglect any wind dependencies.

Pitch.- From equation (A62) the output of the pitch attitude gyro is

$$z_k(1) = \theta = v_k(1) + b(1)$$

In this case it suffices to let

$$y_k(1) = z_k(1) \tag{B1}$$

and then $y_k(1)$ can be modeled as

$$\begin{aligned} y_k(1) &= \theta + v_k(1) \\ &= x_k(1) + v_k(1) \end{aligned} \tag{B2}$$

Accelerations.- The outputs of the body mounted accelerometers are given by equations (A63) - (A66). The first step in pre-processing this measurement is to convert them to stability coordinates according to

$$\begin{aligned} A^F_{x_s} &= z_k(2) \cos \alpha^F_o + z_k(3) \sin \alpha^F_o \\ A^F_{z_s} &= -z_k(2) \sin \alpha^F_o + z_k(3) \cos \alpha^F_o \end{aligned} \tag{B3}$$

where

α_o = trim angle-of-attack

Comparison of the stability axis accelerations in equations (B3) with those in (A65) shows that

$$A_{x_s} = A_{x_s} + e_x$$

$$A_{z_s} = A_{z_s} + e_z \tag{B4}$$

where e_x is an error term due to accelerometer noise $v_k(2)$, bias error $b(2)$, scale factor error s, accelerometer alignment error a, and error $(\alpha_o - \alpha_o^F)$ in the trim angle-of-attack. From equations (A63) and (A64)

$$A^F_{x_s} = U_o \varepsilon_2^T [Ax_k + Bu_k + Dw_k] + qU_o \tan\alpha + g \sin(\theta_o + \theta - \alpha_o)$$

$$A^F_{z_s} = U_o \tan\alpha \varepsilon_2^T [Ax_k + Bu_k + Dw_k] - qU_o - g\cos(\theta_o + \theta - \alpha_o) \tag{B5}$$

$$+ [(1 + u')U_o/\cos^2\alpha]\varepsilon_3^T [Ax_k + Bu_k + Dw_k]$$

Define the observations $y_k(2)$ and $y_k(3)$ as follows:

$$y_k(2) = \frac{1}{U_o^F}\left[A^F_{x_s} - g \sin(\theta_o^F - \alpha_o^F)\right] - \varepsilon_2^T B_F u_k$$

$$y_k(3) = \frac{1}{U_o^F}\left[A^F_{z_s} + g \cos(\theta_o^F - \alpha_o^F)\right] - \varepsilon_3^T B_F u_k \tag{B6}$$

The pre-processor then calculates the observations $y_k(2)$ and $y_k(3)$ from the measurements $z_k(2)$ and $z_k(3)$ using equations (B3) and (B6). From equations (B5) and (B6) these observations can be approximated as linear functions of the states as follows:

$$y_k(2) \approx q \tan \alpha + \varepsilon_2^T A_F x_k + (g/U_o^F) \cos(\theta_o^F - \alpha_o^F) \sin \theta + v_k(2)$$

$$\approx \sum_{j=1}^{6} A_F(2,j) x_k(j) + (g/U_o^F) \cos(\theta_o^F - \alpha_o^F) x_k(1) + v_k(2) \qquad \text{(B7)}$$

$$y_k(3) \approx -q + (\tan \alpha)\ \varepsilon_2^T A_F x_k + [(1 + u')/\cos^2 \alpha] \varepsilon_3^T A_F x_k + v_k(3)$$

$$+ (g/U_o^F) \sin(\theta_o^F - \alpha_o^F) \sin \theta \qquad \text{(B8)}$$

$$\approx -x_k(4) + (g/U_o^F) \sin(\theta_o^F - \alpha_o^F) x_k(1) + \sum_{j=1}^{6} A_F(3,j) x_k(j) + v_k(3)$$

Pitch rate.- From equation (A64) the output of the pitch rate gyro is

$$z_k(4) = q + v_k(4)$$

It is sufficient to let

$$y_k(4) = z_k(4) \qquad \text{(B9)}$$

in which case $y(4)$ can be modeled as

$$y_k(4) = x_k(4) + v_k(4) \qquad \text{(B10)}$$

Air speed.- From equation (A68) the air speed measurement is

$$z_k(5) = V_a[1 + v_k(5)] + b(5)$$

$$= U_o[(1 + u' + u'_W)/\cos(\alpha + \alpha_W)] \cdot [1 + v_k(5)] + b(5)$$

Define the air speed observation as

$$y_k(5) = [z_k(5)/U_o^F] - 1 \qquad \text{(B11)}$$

The observation can be approximated as a linear combination of the states as follows:

$$y_k(5) = \left[\frac{1 + u' + u'_w}{\cos(\alpha + \alpha_w)}\right][1 + v_k(5)] + \frac{b(5)}{U_o^F} - 1$$

$$\approx u' + v_k(5) \tag{B12}$$

$$\approx x_k(2) + v_k(5)$$

Altitude rate.- From equation (A69) the altitude rate measurement is

$$z_k(6) = \dot{h} + v_k(6)$$

$$= U_o(1 + u'_k)[\sin(\theta_o + \theta - \alpha_o) - \tan\alpha\cos(\theta_o + \theta - \alpha_o)] + v_k(6)$$

Define the observation

$$y_k(6) = [z_k(6)/U_o^F] - (\theta_o^F - \alpha_o^F) \tag{B13}$$

which can be approximately modeled as

$$y_k(6) \approx (1 + u')[\sin(\theta_o^F - \alpha_o^F)\cos\theta + \cos(\theta_o^F - \alpha_o^F)\sin\theta$$

$$- \tan\alpha\cos(\theta_o^F - \theta_o^F)\cos\theta + \tan\alpha\sin(\theta_o^F - \alpha_o^F)\sin\theta]$$

$$+ v_k(6)/U_o^F - (\theta_o^F - \alpha_o^F) \tag{B14}$$

$$\approx u'\sin(\theta_o^F - \alpha_o^F) + \cos(\theta_o^F - \alpha_o^F)\theta - \alpha + v_k(6)$$

$$\approx (\theta_o^F - \alpha_o^F)x_k(2) + x_k(1) - x_k(3) + v_k(6)$$

Angle-of-attack.- From equation (A70) the output of the angle-of-attack sensor is

$$z_k(7) = \alpha + \alpha_W + v_k(7) + b(7)$$

Define the observation

$$y_k(7) = z_k(7)$$

which can be modeled by

$$\begin{aligned} y_k(7) &= \alpha + \alpha_W + v_k(7) \\ &\approx x_k(3) + v_k(7) \end{aligned} \tag{B16}$$

The pre-processor computes the observations y_k from the measurements z_k according to equations (B1), (B3), (B6), (B9), (B11), (B13), and (B15). These observations are the inputs to the failure detection filter. For use in the filter algorithms the observations can now be expressed as in equation (35) with the observation matrix defined by equation (B17).

$$H_F = \begin{bmatrix} 1 & 0 & 0 & 0 & 0 & 0 \\ A_F(2,1) + g/U_o^F \cos\left(\theta_o^F - \alpha_o^F\right) & A_F(2,2) & A_F(2,3) & A_F(2,4) & A_F(2,5) & A_F(2,6) \\ A_F(3,1) + g/U_o^F \sin\left(\theta_o^F - \alpha_o^F\right) & A_F(3,2) & A_F(3,3) & A_F(3,4) - 1 & A_F(3,5) & A_F(3,6) \\ 0 & 0 & 0 & 1 & 0 & 0 \\ 0 & 1 & 0 & 0 & 0 & 0 \\ 1 & \left(\theta_o^F - \alpha_o^F\right) & 0 & 0 & 0 & 0 \\ 0 & 0 & 1 & 0 & 0 & 0 \end{bmatrix}$$

REFERENCES

1. Willsky, Alan S.: A Survey of Design Methods for Failure Detection in Dynamic Systems. Automatica, vol. 12, 1976, pp. 601-611.

2. Chow, Edward Y.: Failure Detection System Design Methodology. LIDS-TH-1055, Lab. for Info. and Decision Sciences, MIT, Oct. 1980.

3. Chow, Edward Y.; and Willsky, Alan S.: Issues in the Development of a General Design Algorithm for Reliable Failure Detection. 19th IEEE Conf. on Decision and Cont., 1980, pp. 1006-1012.

4. Motyka, Paul; Landey, M.; and McKern, R.: Failure Detection and Isolation Analysis of a Redundant Strapdown Inertial Measurement Unit. (R-1414, C. S. Draper Lab.; NAS1-15933.) NASA CR-165658, Feb. 1981.

5. Deyst, J., et al.: Development and Testing of Advanced Redundancy Management Methods for the F-8 DFBW Aircraft. 1977 IEEE Conf. on Decision and Cont., pp. 309-315.

6. Caglayan, Alper K.; and Lancraft, Roy E.: An Aircraft Sensor Fault Tolerant System. (Rept. No. 4858, Bolt Beranek and Newman; NAS1-16579.) NASA CR-165876, April 1982.

7. Friendland, Bernard: Maximum Likelihood Failure Detection of Aircraft Flight Control Sensors. AIAA 82-4252, J. of Guid., Cont., and Dynamics, vol. 5, no. 5, 1982, pp. 498-503.

8. Willsky, Alan S.; and Jones, Harold L.: A Generalized Likelihood Ratio Approach to State Estimation in Linear Systems Subject to Abrupt Changes. 1974 IEEE Conf. on Decision and Cont., Paper No. FP4.3, pp. 846-853.

9. Chow, Edward; Dunn, Keh-Ping; and Willsky, Alan S.: A Dual-Model Generalized Likelihood Ratio Approach to Self-Reorganizing Digital Flight Control System Design. Research Status Rept. No. 1, Electronic Sys. Lab., MIT, April 14, 1975.

10. Bueno, Ramon, et al.: A Dual-Mode Generalized Likelihood Ratio Approach to Self-Reorganizing Digital Flight Control System Design. (Research Status Rept. No. 2, ESL-IR-642, Electronic Sys. Lab., MIT; NASA Grant NSG-1112.) NASA CR-146386, 1975.

11. Bueno, Ramon A.: Performance and Sensitivity Analysis of the Generalized Likelihood Ratio Method for Failure Detection. (M.S. Thesis, ESL-R-706, Electronic Sys. Lab., MIT; NASA Grant NSG-1112.) NASA CR-149272, 1977.

12. Anon.: A Dual-Mode Generalized Likelihood Approach to Self-Reorganizing Digital Flight Control System Design. (ESL-FR-707, Electronic Sys. Lab., MIT; NASA Grant NSG-1112.) NASA CR-149317, 1977.

13. Liu, Jack S.; and Jones, Harold L.: Linear Manifold Constrained GLR. IEEE Trans. Auto. Cont., vol. AC-22, no. 6, Dec. 1977, pp. 988-989.

14. Chang, C. B.; and Dunn, K. P.: On GLR Detection and Estimation of Unexpected Inputs in Linear Discrete Systems. IEEE Trans. Auto. Cont., vol. AC-24, no. 3, June 1979, pp. 499-501.

15. Tylee, J. Louis: Bias Identification in PWR Pressurizer Instrumentation Using the Generalized Likelihood Ratio Technique. Paper FA-4B, 1981 Joint Auto. Controls Conf.

16. Beard, Richard V.: Failure Accommodation in Linear Systems Through Self-Reorganization. Ph.D. Thesis, MIT, 1971.

17. Jones, Harold Lee: Failure Detection in Linear Systems. Ph.D. Thesis, MIT, 1973.

18. Meserole, Jere S.: Detection Filters for Fault-Tolerant Control of Turbofan Engines. Ph.D. Thesis, MIT, 1981.

19. Chalk, C. R., et al.: Background Information and User Guide for MIL-F-8785B/ASG/ - Military Specification - Flying Qualities of Piloted Airplanes. Tec. Rept. AFFFDL-TR-69-72, Cornell Aeronautical Lab., August 1969.

20. Halyo, Nesim: Development of an Optimal Automatic Control Law and Filter Algorithm for Steep Glideslope Capture and Glideslope Tracking. NASA CR-2720, 1976.

21. Ogata, Katsuhiko: State Space Analysis of Control Systems. Prentice Hall, Inc., 1967.

TABLE III.- FAILURE DETECTION PERFORMANCE WITH AN EIGENVALUE OF 0.9 AND THRESHOLDS SET AT HEAVY TURBULENCE LEVEL

Failure		Turbulence			
Type	Magnitude, degrees	None	Medium	Heavy	Thunderstorm
Elevator	10 3 1	 n/n/n/n n/n/n/n	n/n/n/n n/n/n/n n/n/n/n	Y/Y/Y/Y Y/n/n/n	Y/Y/Y/Y
Throttle	40 12 4			Y/Y/Y/Y	
Stabilizer	-6 3 -1			Y/Y/Y/Y	
Spoiler	8 3 1			Y/Y/Y/Y	

Y/Y/Y/Y indicates detection using the 30-, 20-, 10-, and 1-sample windows.

n indicates failure not detected.

TABLE IV.- FAILURE DETECTION PERFORMANCE WITH AN EIGENVALUE OF 0.5 AND THRESHOLDS SET AT HEAVY TUBULENCE LEVEL

Failure		Turbulence			
Type	Magnitude, degrees	None	Medium	Heavy	Thunderstorm
Elevator	10	n/n/n/n	n/n/n/n	Y/Y/Y/Y	Y/Y/Y/Y
	3	n/n/n/n	n/n/n/n	Y/Y/Y/Y	
	1	n/n/n/n	n/n/n/n	Y/Y/Y/Y	
Throttle	40	n/n/n/n	n/n/n/n	n/Y/Y/Y	
	12			n/Y/Y/Y	
	4	n/n/n/n		n/Y/n/Y	
Stabilizer	-6	n/n/n/n	n/n/n/n	Y/Y/Y/Y	
	3			Y/Y/Y/Y	
	-1	n/n/n/n		Y/Y/Y/Y	
Spoiler	8	n/n/n/n	n/n/n/n	Y/Y/Y/Y	
	3			Y/Y/Y/Y	
	1	n/n/n/n		Y/Y/Y/Y	

Y/Y/Y/Y indicates detection using the 30-, 20-, 10-, and 1-sample windows.

n indicates failure not detected.

TABLE V.- FAILURE DETECTION PERFORMANCE WITH AN EIGENVALUE OF 0.5 AND THRESHOLDS SET AT NO TURBULENCE LEVEL

Failure		Turbulence			
Type	Magnitude, degrees	None	Medium	Heavy	Thunderstorm
Elevator	10 3 1	n/n/n/Y n/n/n/Y	Y/Y/Y/Y	Y/Y/Y/Y Y/Y/Y/Y Y/Y/Y/Y	Y/Y/Y/Y
Throttle	40 12 4	Y/n/n/n n/n/n/n	Y/Y/Y/Y	Y/Y/Y/Y Y/Y/Y/Y Y/Y/Y/Y	
Stabilizer	-6 3 -1	Y/Y/Y/Y n/n/n/n	Y/Y/Y/Y	Y/Y/Y/Y Y/Y/Y/Y Y/Y/Y/Y	
Spoiler	8 3 1	Y/Y/Y/Y Y/Y/Y/Y	Y/Y/Y/Y	Y/Y/Y/Y Y/Y/Y/Y Y/Y/Y/Y	

Y/Y/Y/Y indicates detection using the 30-, 20-, 10-, and 1-sample windows.

n indicates failure not detected.

TABLE VI.- FAILURE IDENTIFICATION PERFORMANCE WITH AN EIGENVALUE OF 0.9: FAILURE CORRECTLY IDENTIFIED

Failure		Turbulence			
Type	Magnitude, degrees	None	Medium	Heavy	Thunderstorm
Elevator	10		*/*/*/*	$\hat{i}$:Y/Y/Y/Y $\bar{i}$:Y/n/n/Y	$\hat{i}$:Y/Y/Y/Y $\bar{i}$:n/n/n/n
	3	*/*/*/*	*/*/*/*	$\hat{i}$:Y/*/*/* $\bar{i}$:n/*/*/*	
	1	*/*/*/*	*/*/*/*		
Throttle	40			$\hat{i}$:n/n/n/n $\bar{i}$:Y/Y/Y/Y	
	12				
	4				
Stabilizer	-6			$\hat{i}$:n/n/n/n $\bar{i}$:n/n/n/n	
	3				
	-1				
Spoiler	8			$\hat{i}$:n/n/n/n $\bar{i}$:n/n/n/n	
	3				
	1				

Y/Y/Y/Y indicates correct identification using the 30-, 20-, 10-, and 1-sample data windows.

n indicates failure not correctly identified.

$\hat{i}$ indicates identification based on maximum value of correlation.

$\bar{i}$ indicates identification based on maximum value of normalized correlation.

* indicates failure not detected.

TABLE VII.- FAILURE IDENTIFICATION PERFORMANCE WITH AN EIGENVALUE OF 0.5: FAILURE CORRECTLY IDENTIFIED

Failure		Turbulence			
Type	Magnitude, degrees	None	Medium	Heavy	Thunderstorm
Elevator	10	*/*/*/*	*/*/*/*	$\hat{i}$:Y/Y/Y/Y $\bar{i}$:n/n/n/n	$\hat{i}$:Y/Y/Y/Y $\bar{i}$:n/n/n/n
	3	*/*/*/*	*/*/*/*	$\hat{i}$:Y/Y/Y/Y $\bar{i}$:n/n/Y/n	
	1	*/*/*/*	*/*/*/*	$\hat{i}$:Y/Y/Y/Y $\bar{i}$:n/Y/Y/n	
Throttle	40	*/*/*/*	*/*/*/*	$\hat{i}$:*/n/n/n $\bar{i}$:*/n/n/Y	
	12			$\hat{i}$:*/n/n/n $\bar{i}$:*/n/n/Y	
	4	*/*/*/*		$\hat{i}$:*/n/*/n $\bar{i}$:*/n/*/Y	
Stabilizer	-6	*/*/*/*	*/*/*/*	$\hat{i}$:n/n/n/n $\bar{i}$:n/n/n/n	
	3			$\hat{i}$:n/n/n/n $\bar{i}$:Y/Y/n/Y	
	-1	*/*/*/*		$\hat{i}$:n/n/n/n $\bar{i}$:n/n/n/n	
Spoiler	8	*/*/*/*	*/*/*/*	$\hat{i}$:n/n/n/n $\bar{i}$:n/n/n/n	
	3			$\hat{i}$:n/n/n/n $\bar{i}$:n/n/n/n	
	1	*/*/*/*		$\hat{i}$:n/n/n/n $\bar{i}$:n/n/n/n	

Y/Y/Y/Y indicates correct identification using the 30-, 20-, 10-, and 1-sample data windows.

n indicates failure not correctly identified.

$\hat{i}$ indicates identification based on maximum value of correlation.

$\bar{i}$ indicates identification based on maximum value of normalized correlation.

* indicates failure not detected.

TABLE VIII.- NORMALIZED CORRELATIONS FOR A 20-SAMPLE WINDOW WITH AN EIGENVALUE OF 0.9

Failure		Turbulence			
Type	Magnitude, degrees	None	Medium	Heavy	Thunderstorm
Elevator	10		0.602	1.106	2.327
			.198	.557	3.073
			.605	1.115	2.382
			.598	1.102	2.320
	3	0.152	.484	.956	
		.098	.357	.886	
		.150	.483	.956	
		.153	.484	.959	
	1	.127	.453		
		.094	.388		
		.125	.451		
		.127	.454		
Throttle	40			0.872	
				1.015	
				.869	
				.877	
	12				
	4				
Stabilizer	-6			0.818	
				1.159	
				.807	
				.824	
	3				
	-1				
Spoiler	8			1.009	
				1.604	
				1.005	
				1.014	
	3				
	1				

Values listed in order of c_1^*, c_2^*, c_3^*, c_4^*.

TABLE IX.- NORMALIZED CORRELATIONS FOR A 20-SAMPLE WINDOW WITH AN EIGENVALUE OF 0.5

Failure		Turbulence			
Type	Magnitude, degrees	None	Medium	Heavy	Thunderstorm
Elevator	10		0.506	1.041	2.818
			.394	.870	2.970
			.511	1.047	2.823
			.499	1.032	2.799
	3	0.123	.465	1.014	
		.108	.412	.960	
		.122	.468	1.015	
		.123	.460	1.007	
	1	.110	.452	1.005	
		.099	.414	.984	
		.108	.454	1.005	
		.110	.447	.998	
Throttle	40		0.453	1.007	
			.375	.968	
			.455	1.005	
			.448	1.001	
	12			1.001	
				.987	
				1.000	
				.995	
	4			1.000	
				.993	
				.999	
				.994	
Stabilizer	-6		0.444	0.986	
			.446	1.046	
			.442	.979	
			.441	.981	
	3			1.008	
				.969	
				1.010	
				1.002	
	-1			.997	
				1.004	
				.996	
				.992	
Spoiler	8		0.715	1.238	
			.746	1.377	
			.713	1.232	
			.709	1.231	
	3			1.091	
				1.113	
				1.088	
				1.084	
	1			1.031	
				1.041	
				1.029	
				1.024	

Values listed in order of c_1^*, c_2^*, c_3^*, c_4^*.

TABLE X.- FAILURE DETECTION PERFORMANCE WITH LINEAR MEASUREMENTS AND THRESHOLDS SET AT NO TURBULENCE LEVEL

Failure		Turbulence			
Type	Magnitude, degrees	None	Medium	Heavy	Thunderstorm
Elevator	10	Y/Y/Y/Y	Y/Y/Y/Y	Y/Y/Y/Y #Y/Y/Y/Y	
	3 1	n/n/n/n		Y/Y/Y/Y #Y/Y/Y/Y	
Throttle	40	n/n/n/n	Y/Y/Y/n	Y/Y/Y/Y #Y/Y/Y/Y	
	12 4	n/n/n/n		Y/Y/Y/Y #Y/Y/Y/Y	
Stabilizer	-6	n/n/n/n	Y/Y/Y/n	Y/Y/Y/Y #Y/Y/Y/Y	
	3 -1	n/n/n/n		Y/Y/Y/Y #Y/Y/Y/Y	
Spoiler	8	Y/Y/Y/Y	Y/Y/Y/Y	Y/Y/Y/Y	
	3 1	Y/Y/Y/Y		Y/Y/Y/Y	

Y/Y/Y/Y indicates detection using the 30-, 20-, 10-, and 1-sample windows.

n indicates failure not detected.

no steady state winds.

TABLE XI.- FAILURE DETECTION PERFORMANCE WITH LINEAR MEASUREMENTS AND THRESHOLDS SET AT HEAVY TURBULENCE LEVEL

Failure		Turbulence			
Type	Magnitude, degrees	None	Medium	Heavy	Thunderstorm
Elevator	10	n/n/n/n	n/n/n/n	n/n/n/Y #Y/n/n/Y	
	3 1	n/n/n/n		n/n/n/Y #n/n/n/Y	
Throttle	40	n/n/n/n	n/n/n/n	n/n/n/n #n/n/n/n	
	12 4	n/n/n/n		n/n/n/n #n/n/n/Y	
Stabilizer	-6	n/n/n/n	n/n/n/n	n/n/n/n #n/n/n/n	
	3 -1	n/n/n/n		n/n/n/n #n/n/n/Y	
Spoiler	8	Y/Y/Y/Y	Y/Y/Y/Y	Y/Y/Y/Y	
	3 1	n/Y/Y/Y		Y/Y/Y/Y	

Y/Y/Y/Y indicates detection using the 30-, 20-, 10-, and 1-sample windows.

n indicates failure not detected.

no steady state winds.

TABLE XII.- FAILURE IDENTIFICATION PERFORMANCE WITH LINEAR MEASUREMENTS: FAILURE CORRECTLY IDENTIFIED

Failure		Turbulence			
Type	Magnitude, degrees	None	Medium	Heavy	Thunderstorm
Elevator	10	*/*/*/*	*/*/*/*	$\hat{i}$:*/*/*/n $\bar{i}$:*/*/*/n	
				$\hat{i}$:Y/*/*/n $\bar{i}$:n/*/*/Y	
	3 1	*/*/*/*		$\hat{i}$:*/*/*/n $\bar{i}$:*/*/*/n	
				$\hat{i}$:*/*/*/n $\bar{i}$:*/*/*/Y	
Throttle	40	*/*/*/*	*/*/*/*	*/*/*/* */*/*/*	
	12 4	*/*/*/*		*/*/*/* $\hat{i}$:*/*/*/n $\bar{i}$:*/*/*/n	
Stabilizer	-6	*/*/*/*	*/*/*/*	*/*/*/* */*/*/*	
	3 -1	*/*/*/*		*/*/*/* $\hat{i}$:*/*/*/n $\bar{i}$:*/*/*/n	
Spoiler	8	$\hat{i}$:n/n/n/n $\bar{i}$:n/n/n/n	$\hat{i}$:n/n/n/n $\bar{i}$:n/n/n/n	$\hat{i}$:n/n/n/n $\bar{i}$:n/n/n/n	
	3 1	$\hat{i}$:*/n/n/n $\bar{i}$:*/Y/n/n		$\hat{i}$:n/n/n/n $\bar{i}$:n/n/Y/n	

Y/Y/Y/Y indicates correct identification using the 30-, 20-, 10-, and 1-sample data windows.

n indicates failure not correctly identified.

$\hat{i}$ indicates ID based on maximum value of correlation.

$\bar{i}$ indicates ID based on maximum value of normalized correlation.

* indicates failure not detected.

TABLE XIII.- NORMALIZED CORRELATIONS FOR A 20-SAMPLE DATA WINDOW WITH LINEAR MEASUREMENTS

Failure		Turbulence			
Type	Magnitude, degrees	None	Medium	Heavy	
				w/ss wind	no ss wind
Elevator	10	1.003	1.077	0.921	0.929
		.980	.964	.932	.979
		1.021	1.161	.967	.954
		.998	1.011	.901	.933
	3				
	1	.982		.909	.917
		.966		.923	.970
		.984		.946	.932
		.978		.888	.920
Throttle	40	0.970	1.043	0.903	0.911
		.791	.996	.749	.797
		.976	1.120	.943	.929
		.964	.977	.878	.910
	12				
	4	.979		.908	.916
		.904		.915	.941
		.979		.944	.930
		.975		.887	.918
Stabilizer	-6	0.960	1.034	0.898	0.906
		.957	.954	.923	.971
		.937	1.083	.920	.906
		.960	.972	.877	.909
	3				
	-1	.977		.906	.914
		.963		.922	.969
		.972		.940	.926
		.974		.885	.917
Spoiler	8	3.580	3.654	2.767	
		3.665	3.644	3.428	
		3.494	3.648	2.470	
		3.607	3.620	3.101	
	3				
	1	1.305		1.141	
		1.302		1.204	
		1.294		1.134	
		1.305		1.164	

Values listed in order of c_1^*, c_2^*, c_3^*, c_4^*.
ss = steady state.

TABLE XIV.- VALUES OF STEADY STATE CORRELATION C(J,K) FOR HARDOVER FAILURES

J \ K	1	2	3	4	5	6
1	0.163E-3	-0.996E-4	-0.205E-3	0.495E-1	-0.188E-3	-0.294E-3
2	.355E-5	.104E-2	-.437E-5	-.471E-2	.856E-4	.439E-4
3	.296E-3	.122E-4	-.371E-3	.272E-1	.255E-3	-.923E-4
4	-.101E-3	.123E-3	.127E-3	-.432E-1	.600E-3	.359E-3
5	.762E-4	.893E-4	-.953E-4	-.724E-2	.994E-3	.261E-3
6	-.747E-4	.125E-3	.941E-4	-.387E-1	.713E-3	.364E-3

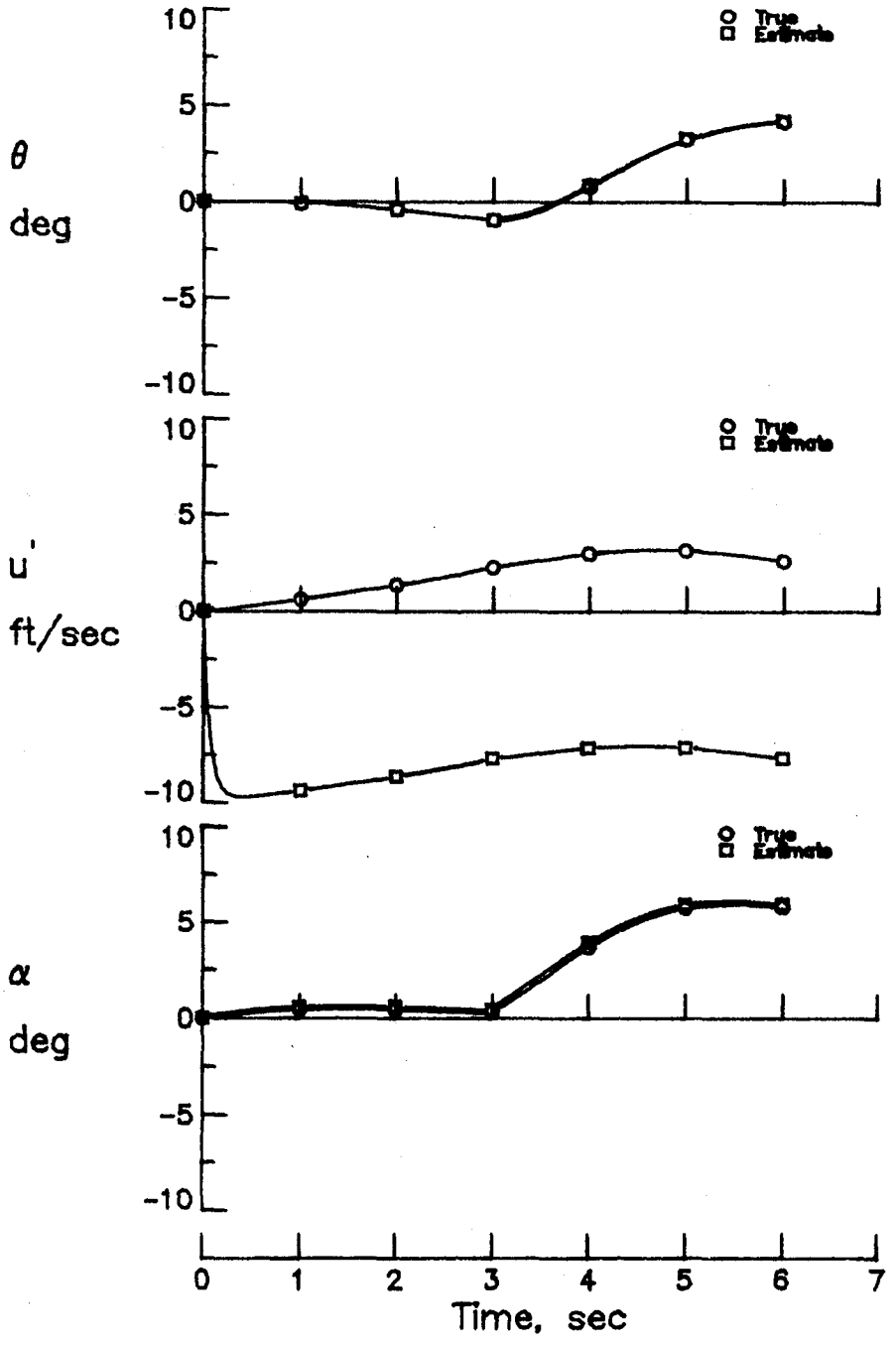

(a) Aircraft states - pitch, velocity, and angle-of-attack.

Figure 1.- Time history plots for an 8 degree spoiler failure at 3 seconds with no turbulence.

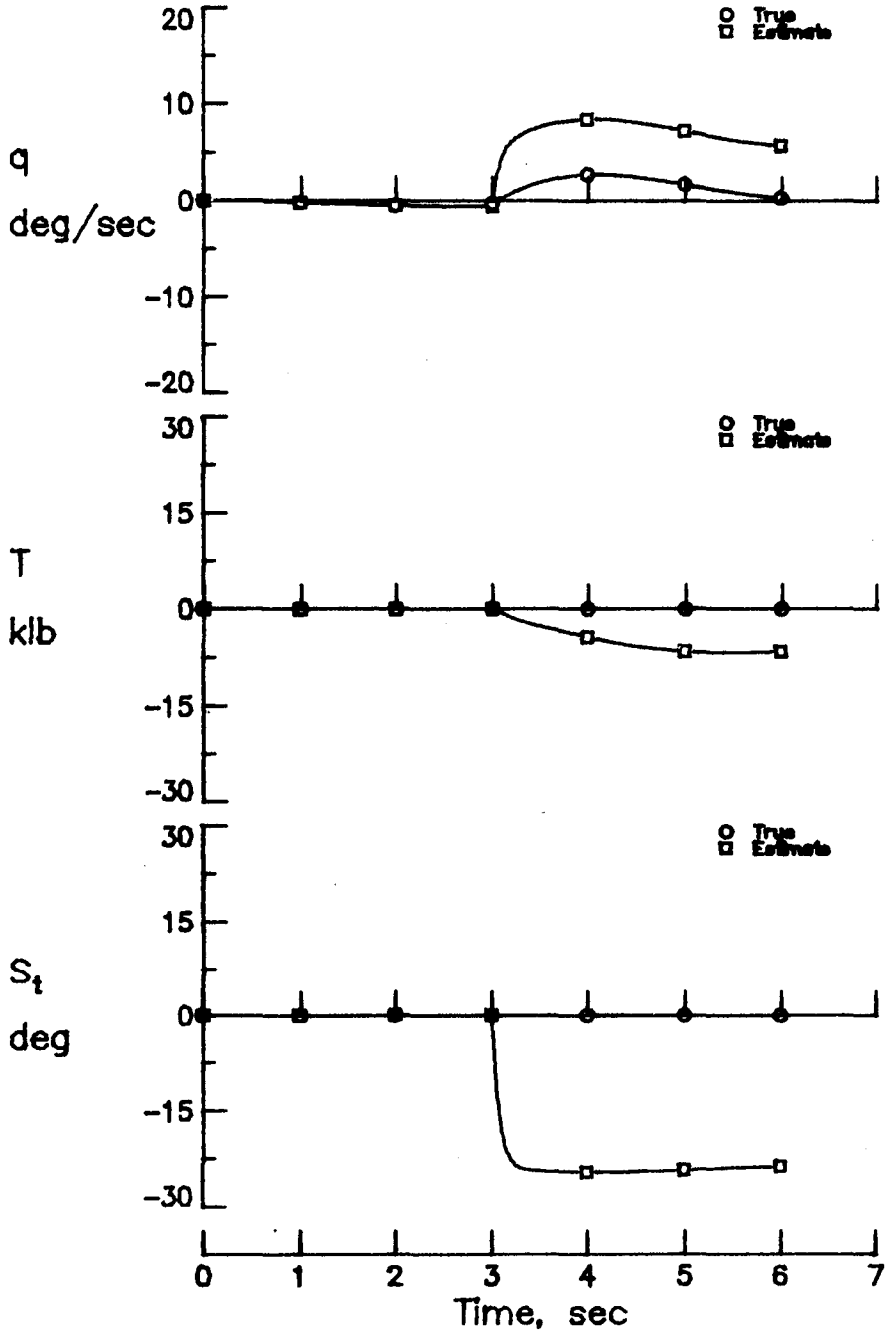

(b) Aircraft states - pitch rate, thrust, and stabilizer.

Figure 1.- Continued.

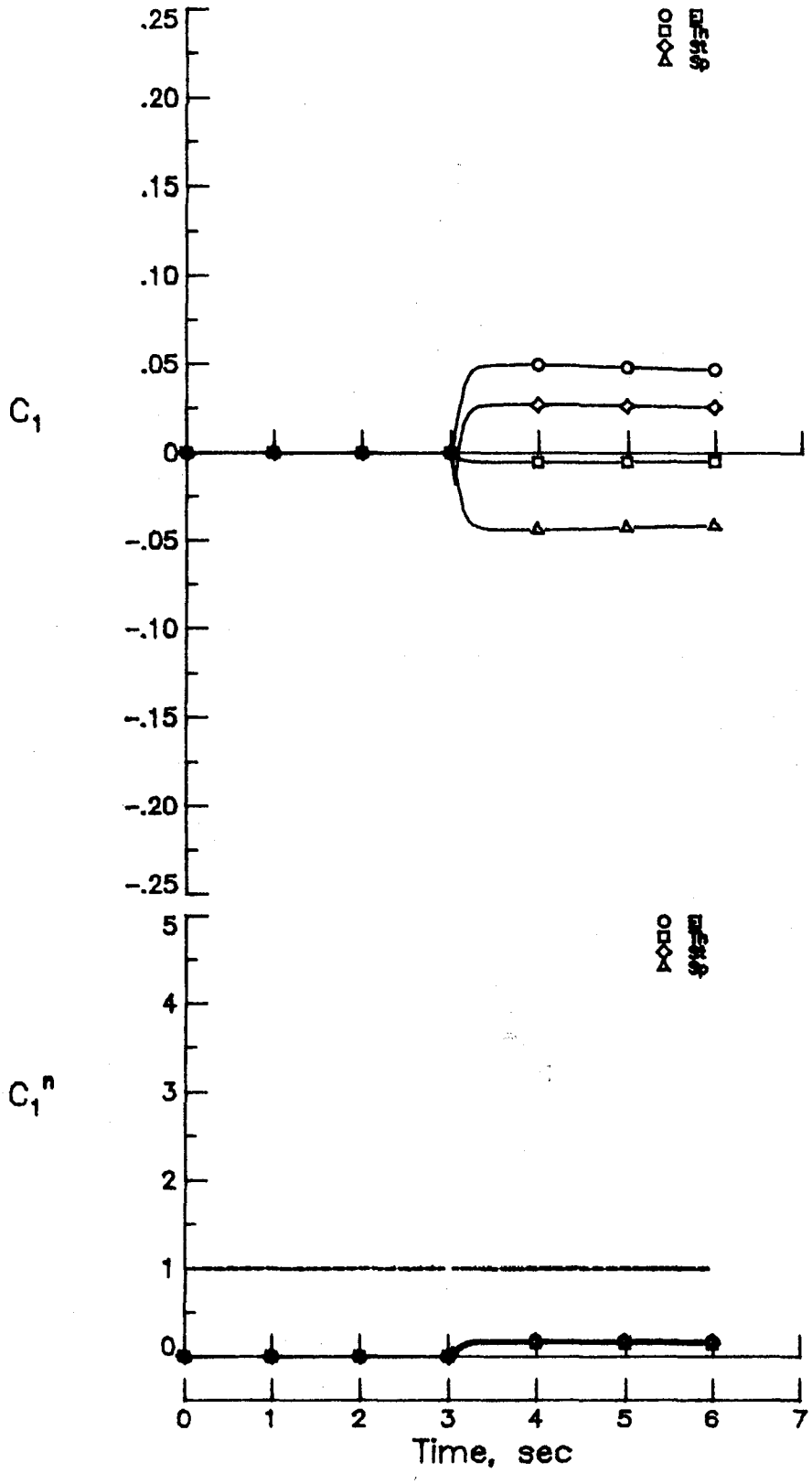

(c) Correlation values for a 1-sample window.

Figure 1.- Continued.

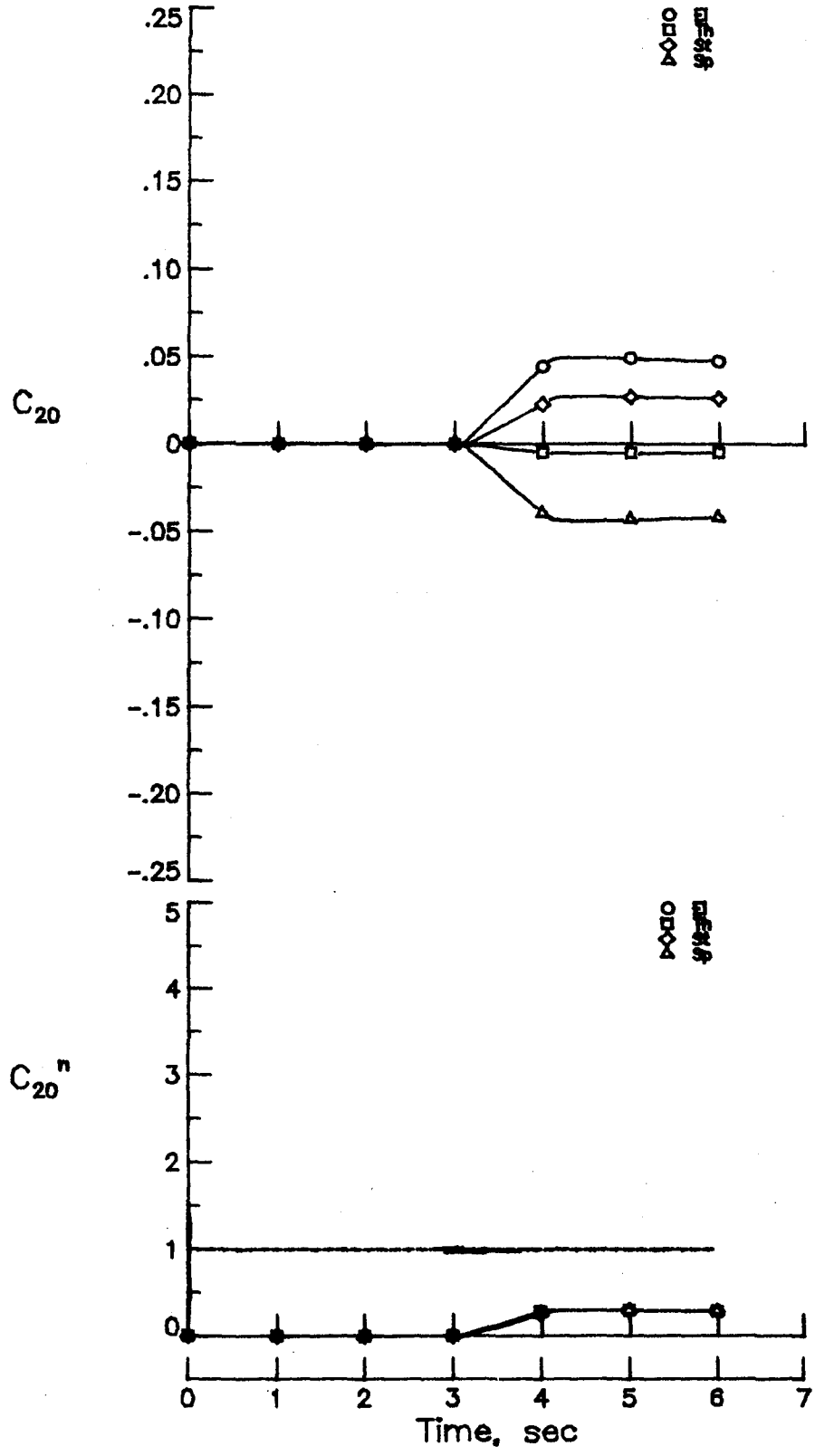

(d) Correlation values for a 20-sample window.

Figure 1.- Continued.

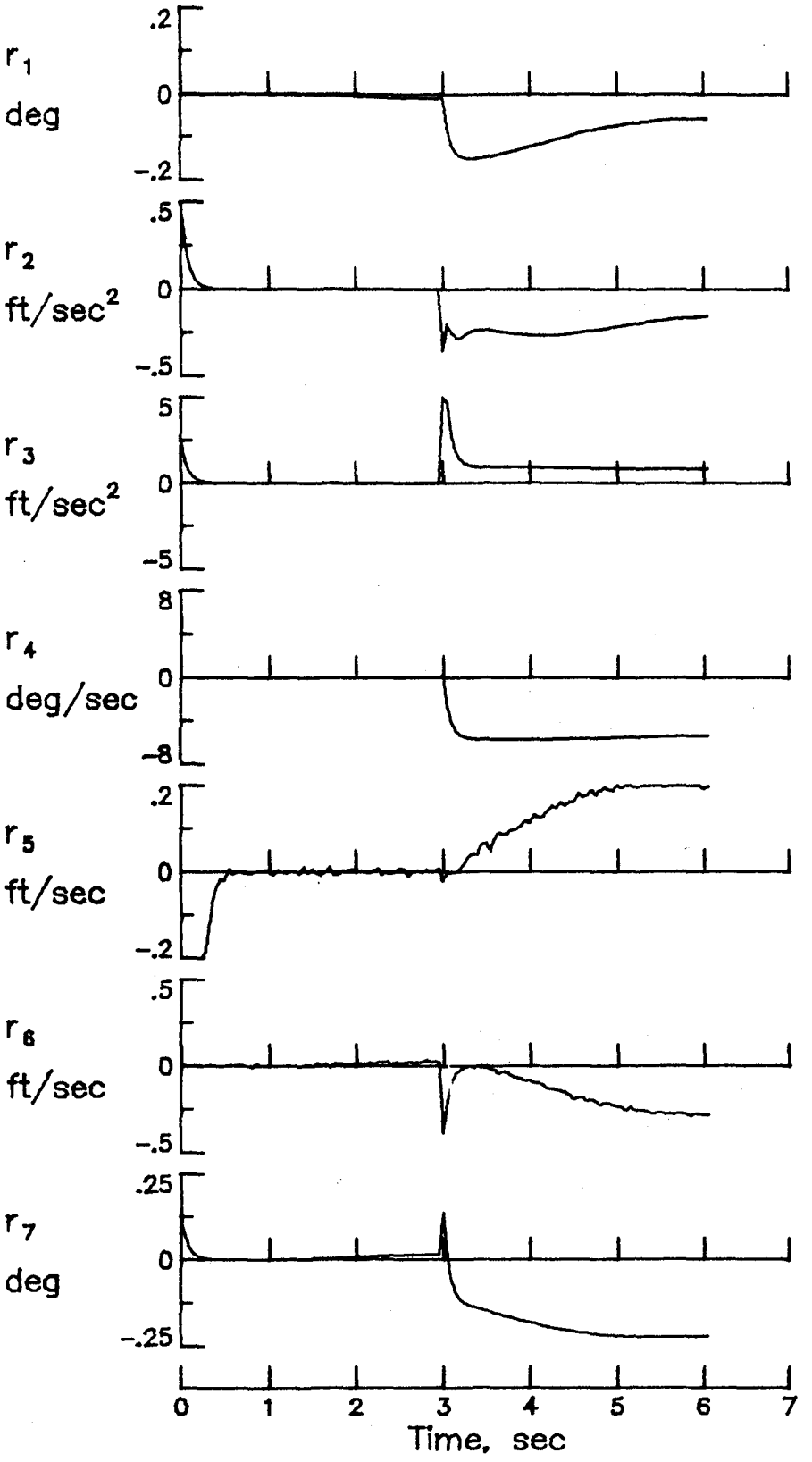

(e) Filter residuals.

Figure 1.- Concluded.

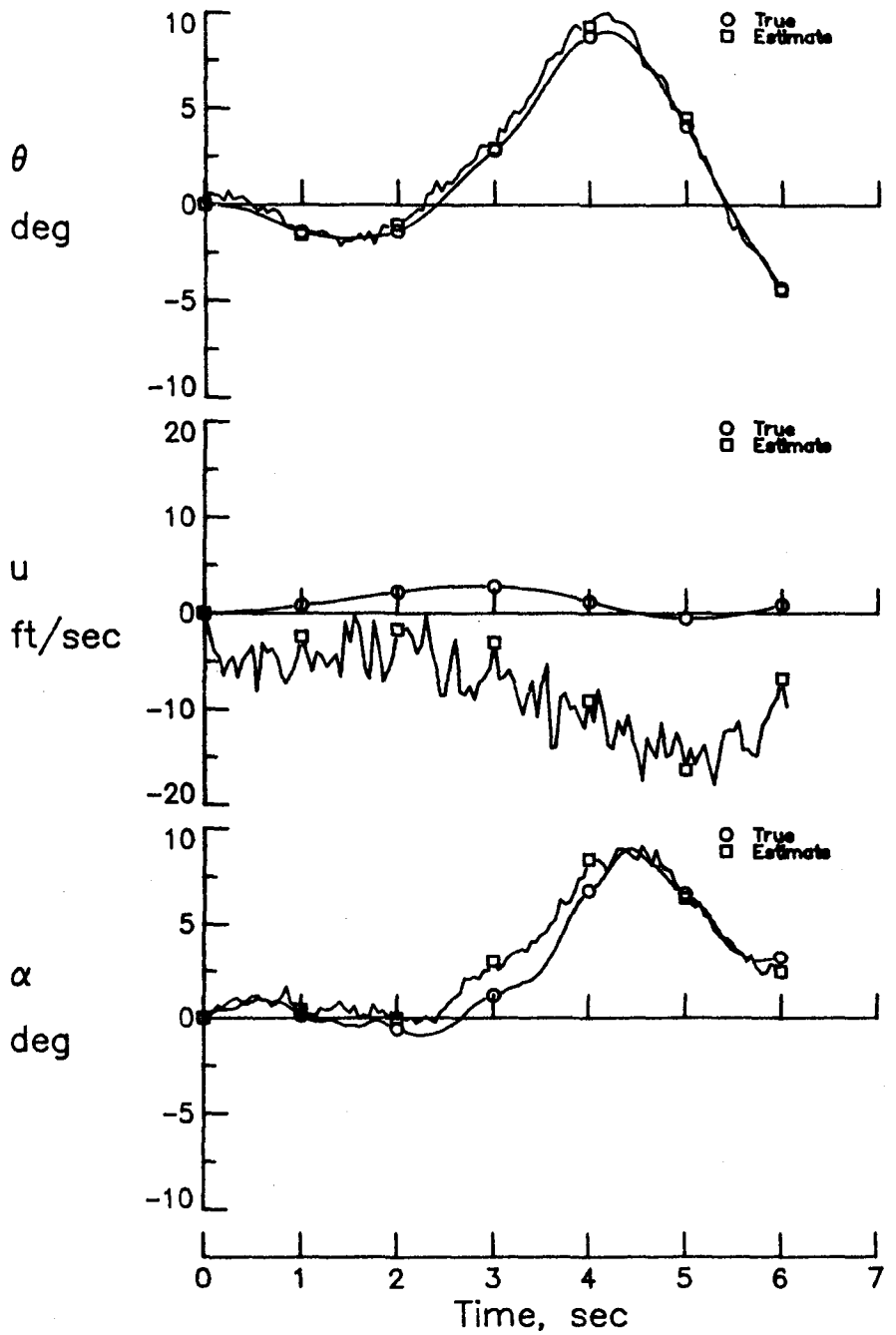

(a) Aircraft states - pitch, velocity, and angle-of-attack.

Figure 2.- Time history plots for an 8 degree spoiler failure at 3 seconds in heavy turbulence.

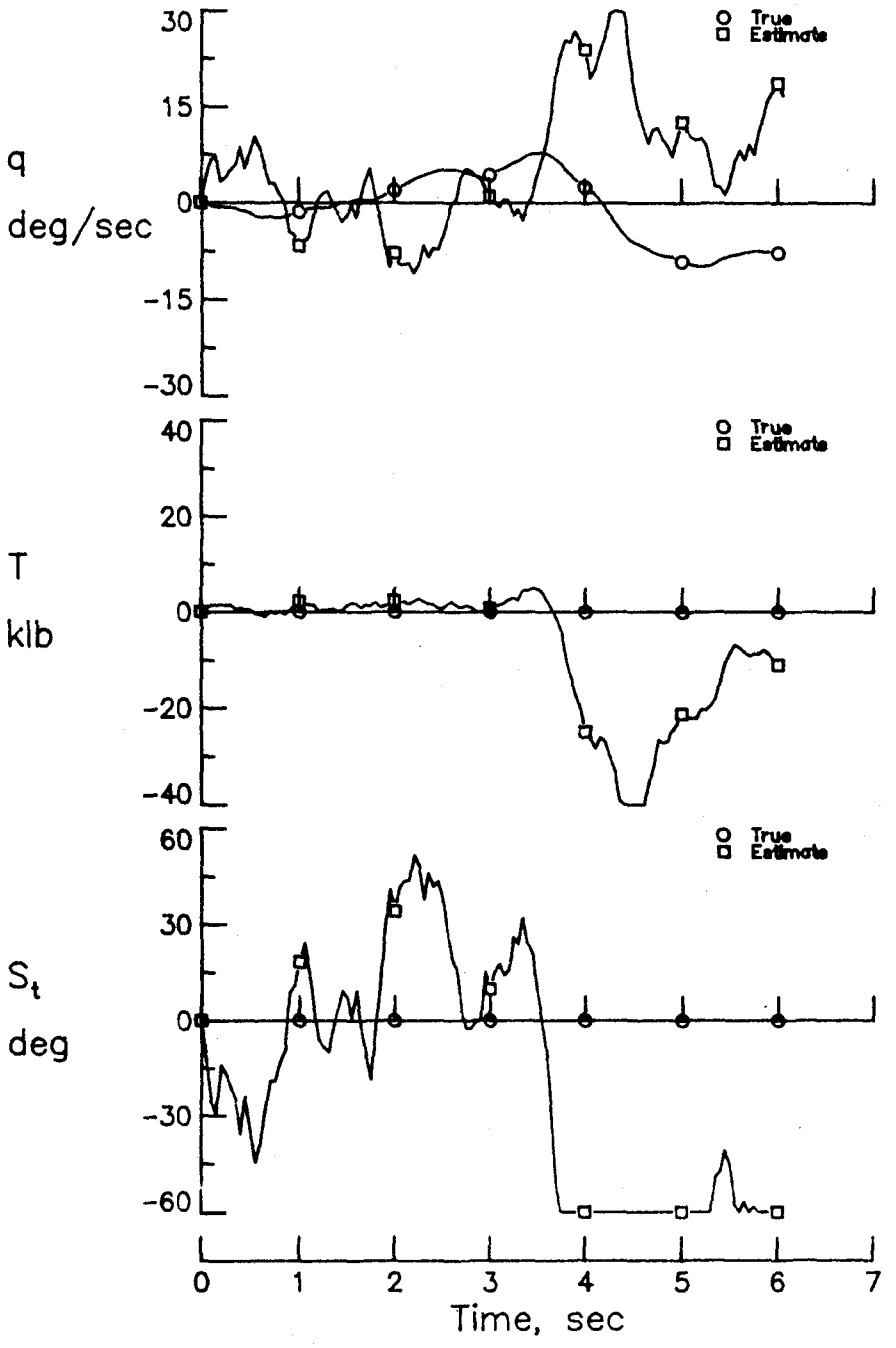

(b) Aircraft states - pitch rate, thrust, and stabilizer.

Figure 2.- Continued.

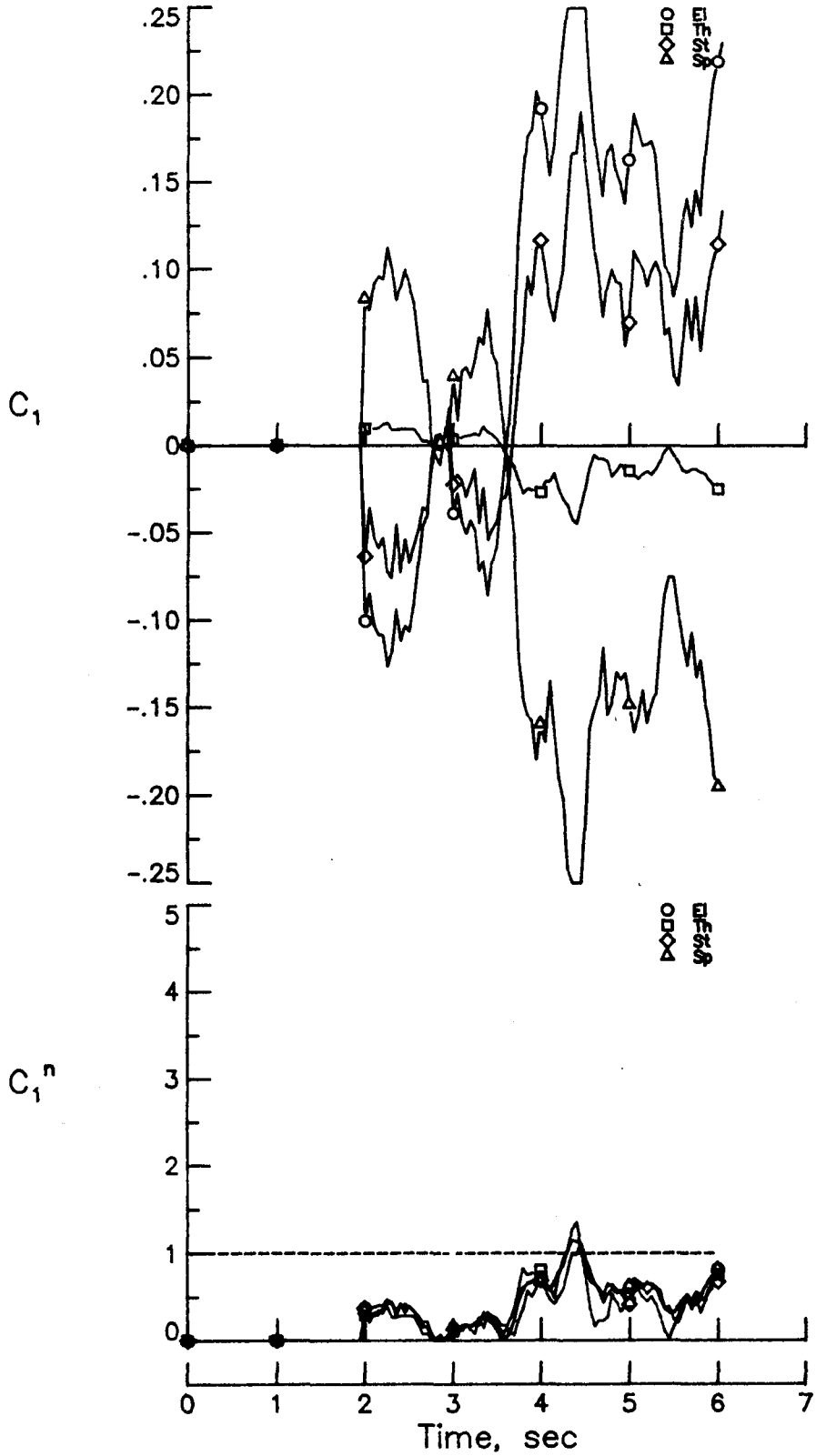

(c) Correlation values for a 1-sample window.

Figure 2.- Continued.

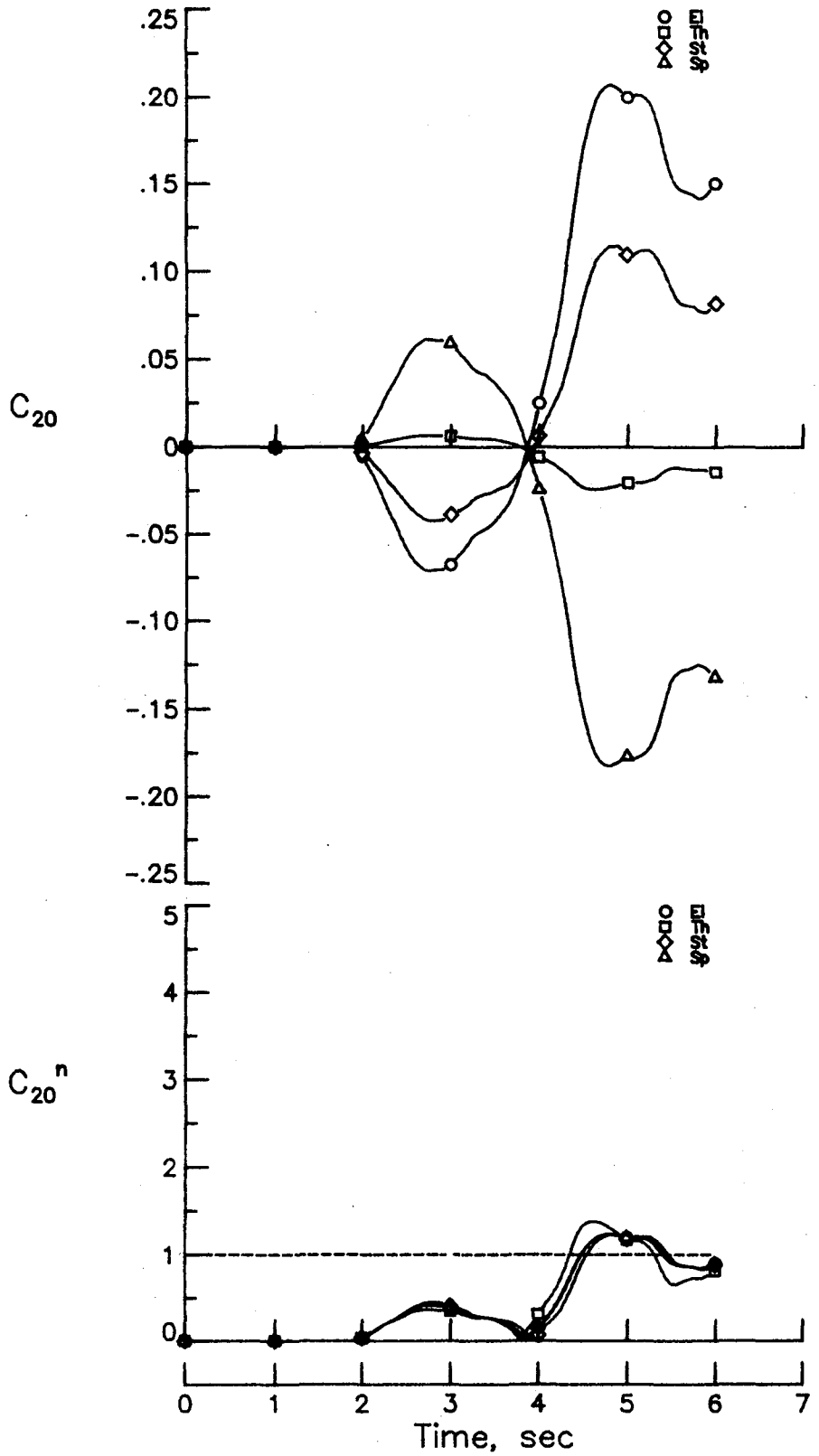

(d) Correlation values for a 20-sample window.

Figure 2.- Continued.

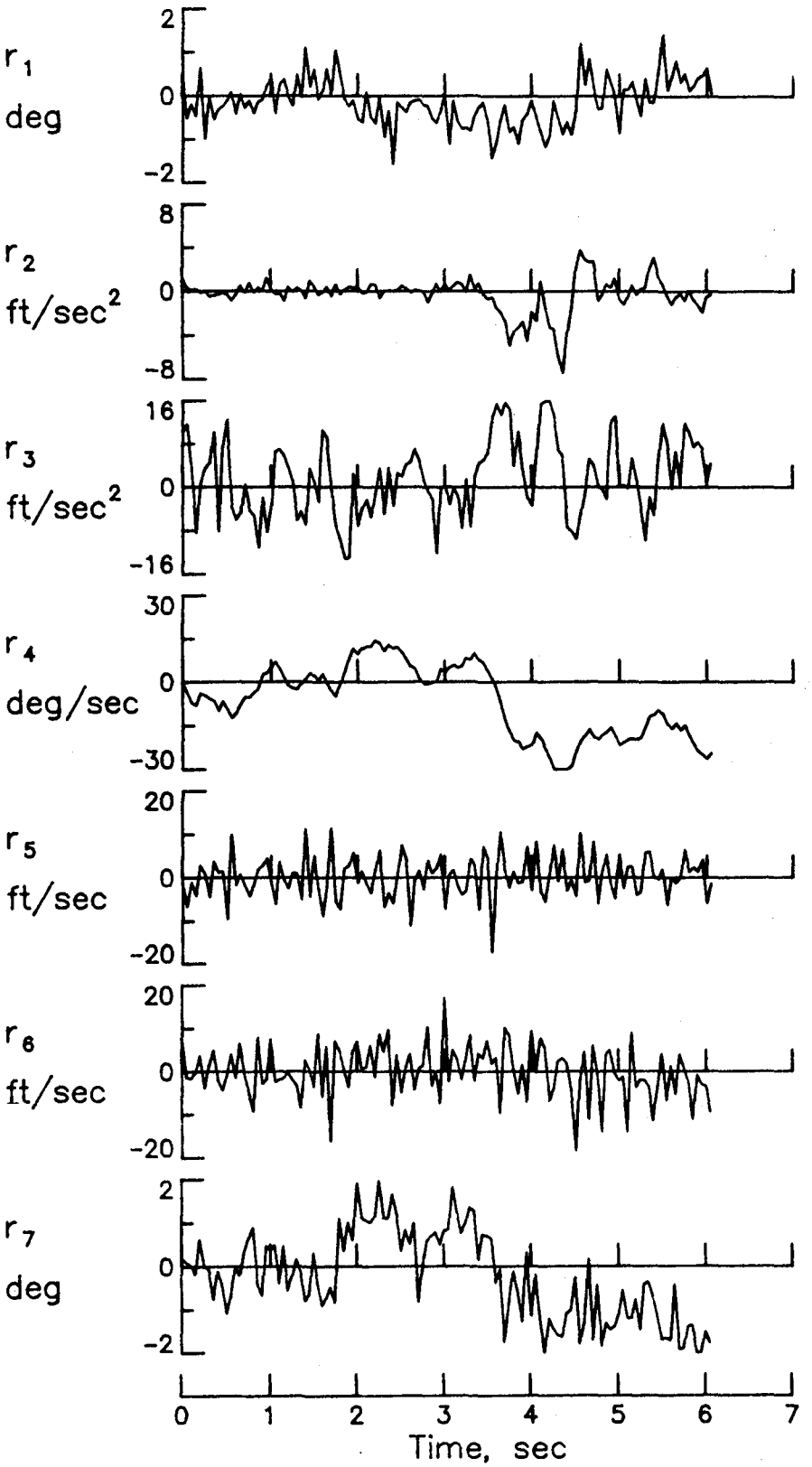

(e) Filter residuals.

Figure 2.- Concluded.

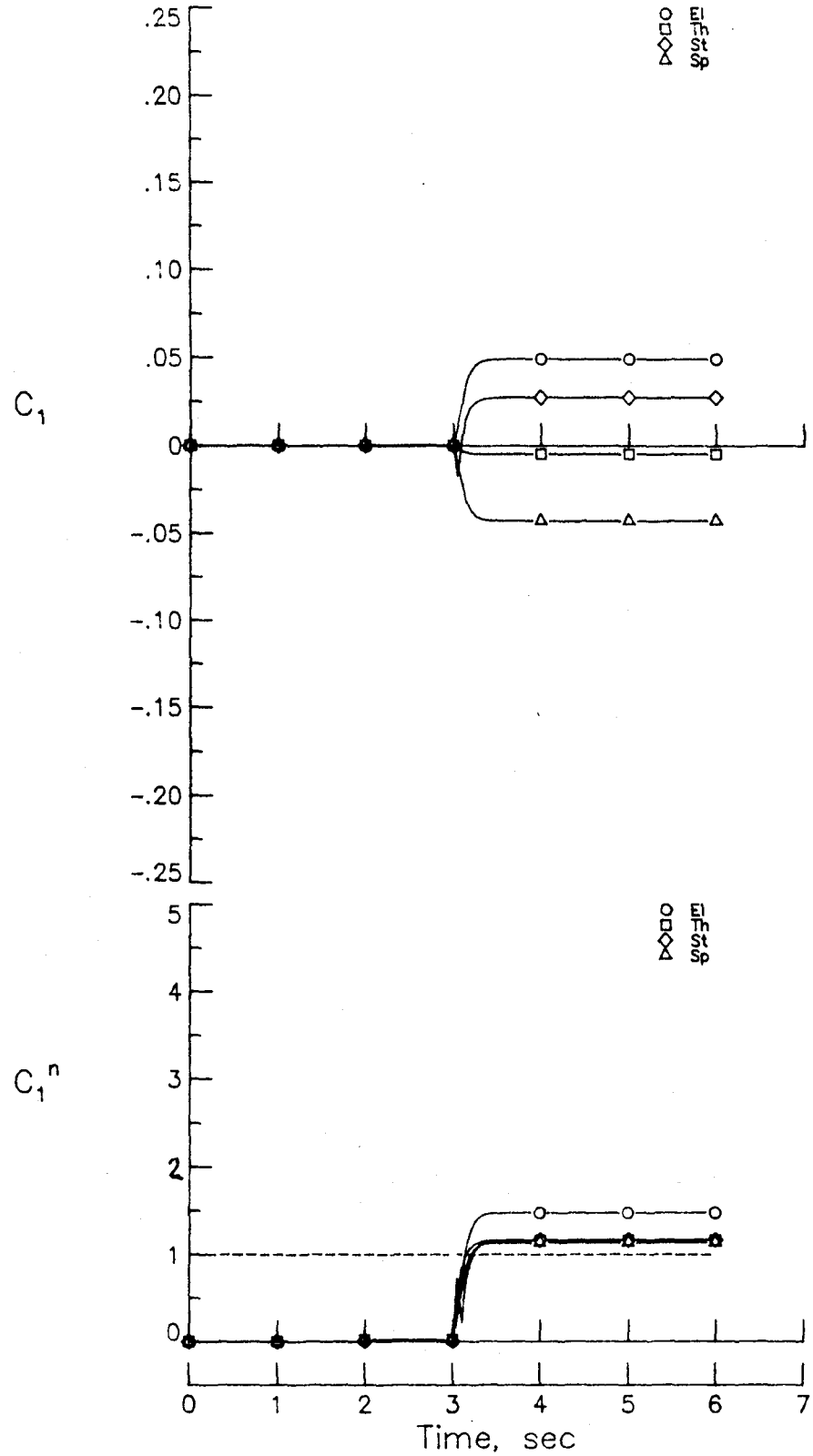

(a) Correlation values for a 1-sample window.

Figure 3.- Time history plots for an 8 degree spoiler failure with linear measurements and no turbulence.

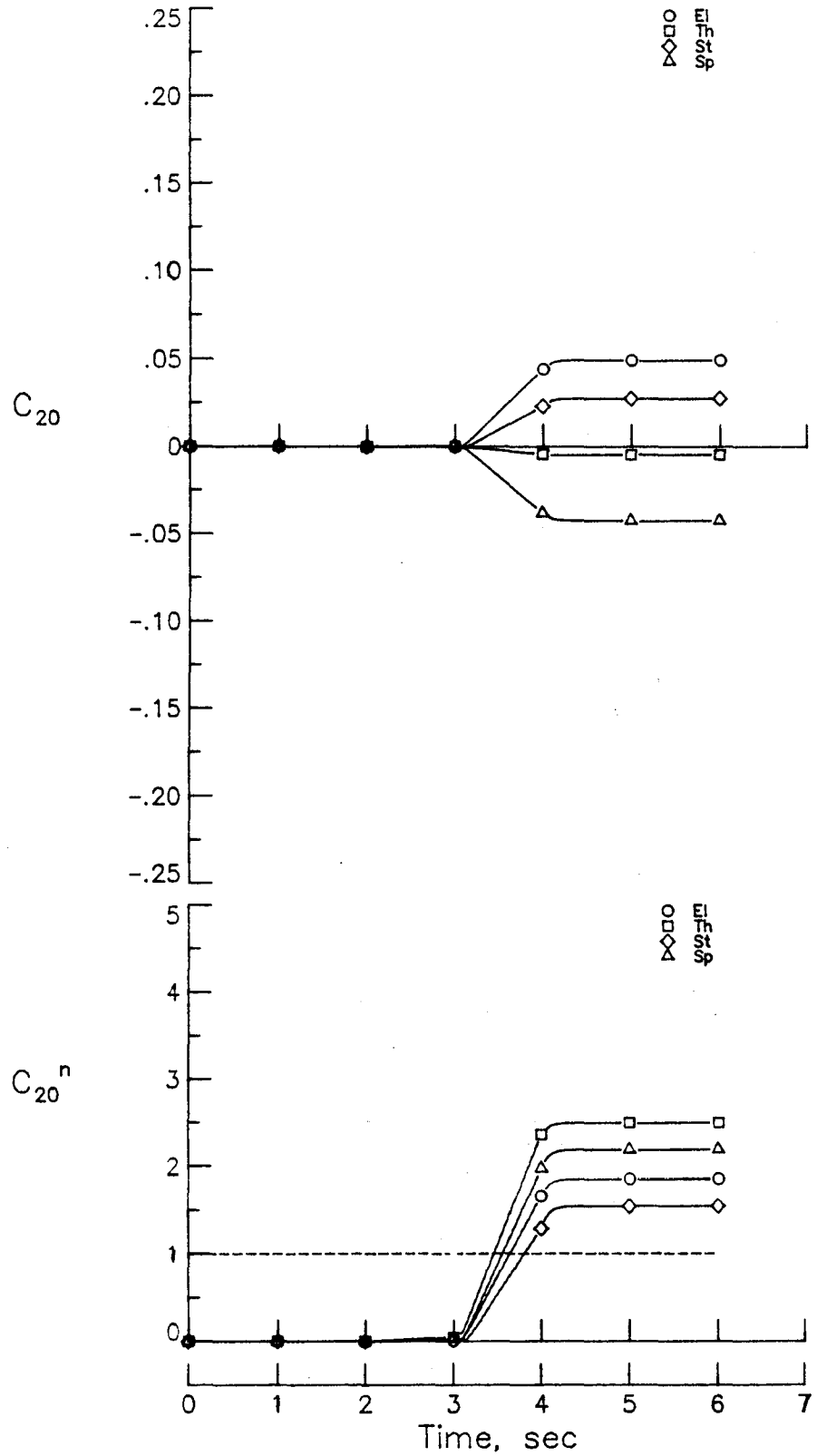

(b) Correlation values for a 20-sample window.

Figure 3.- Continued.

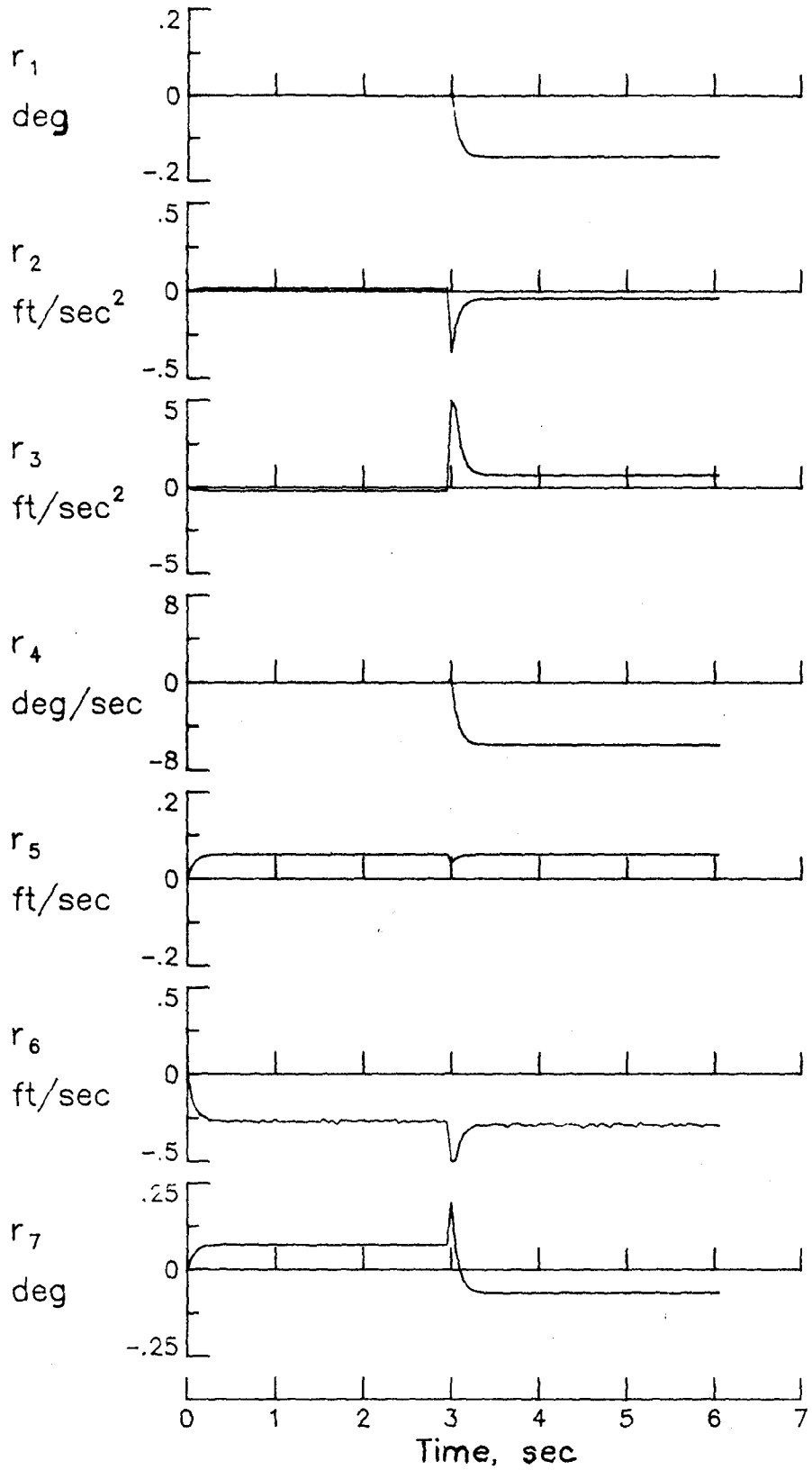

(c) Filter residuals.

Figure 3.- Concluded.

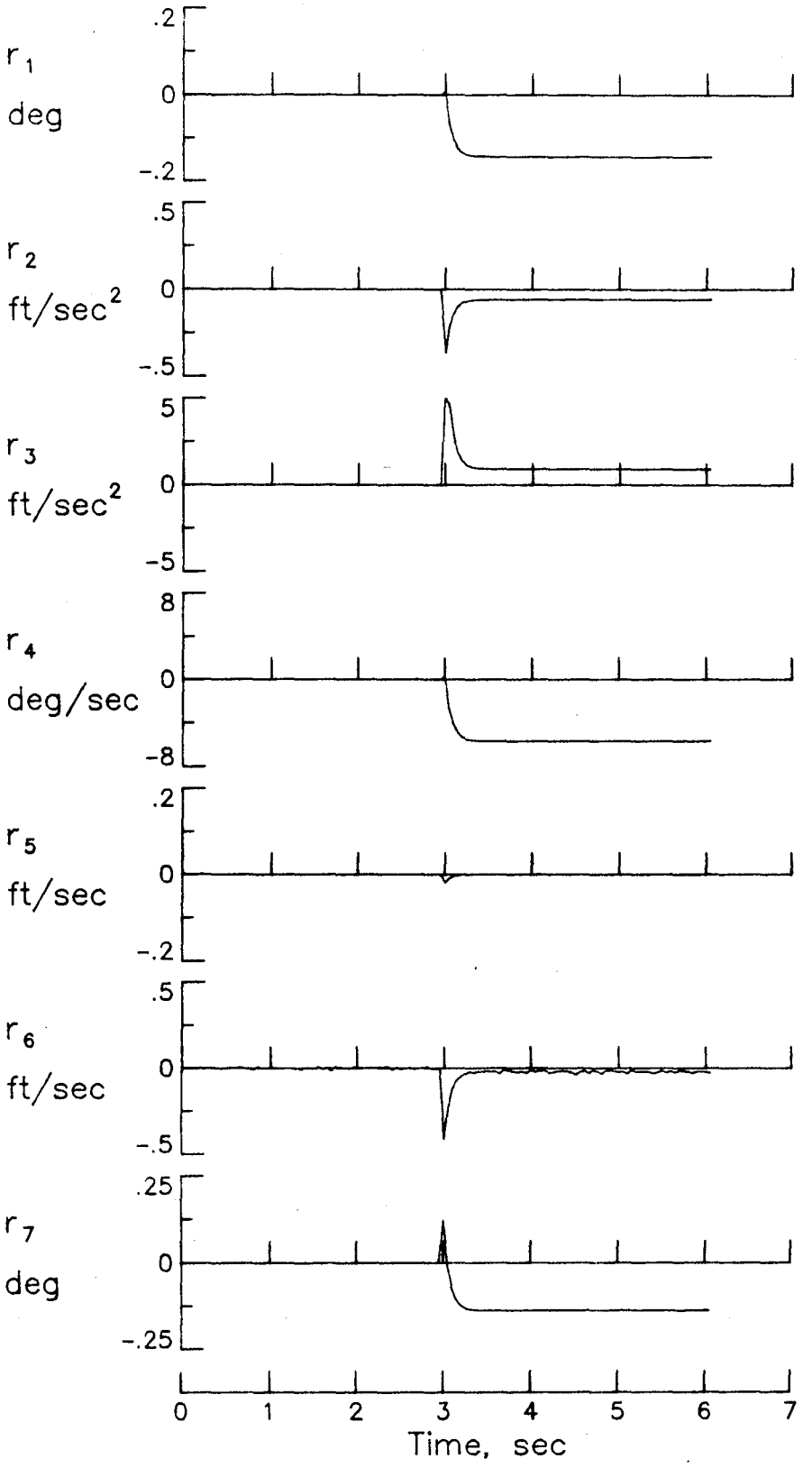

Figure 4.- Filter residuals for an 8 degree spoiler failure with linear measurements, no turbulence, and no steady state winds.

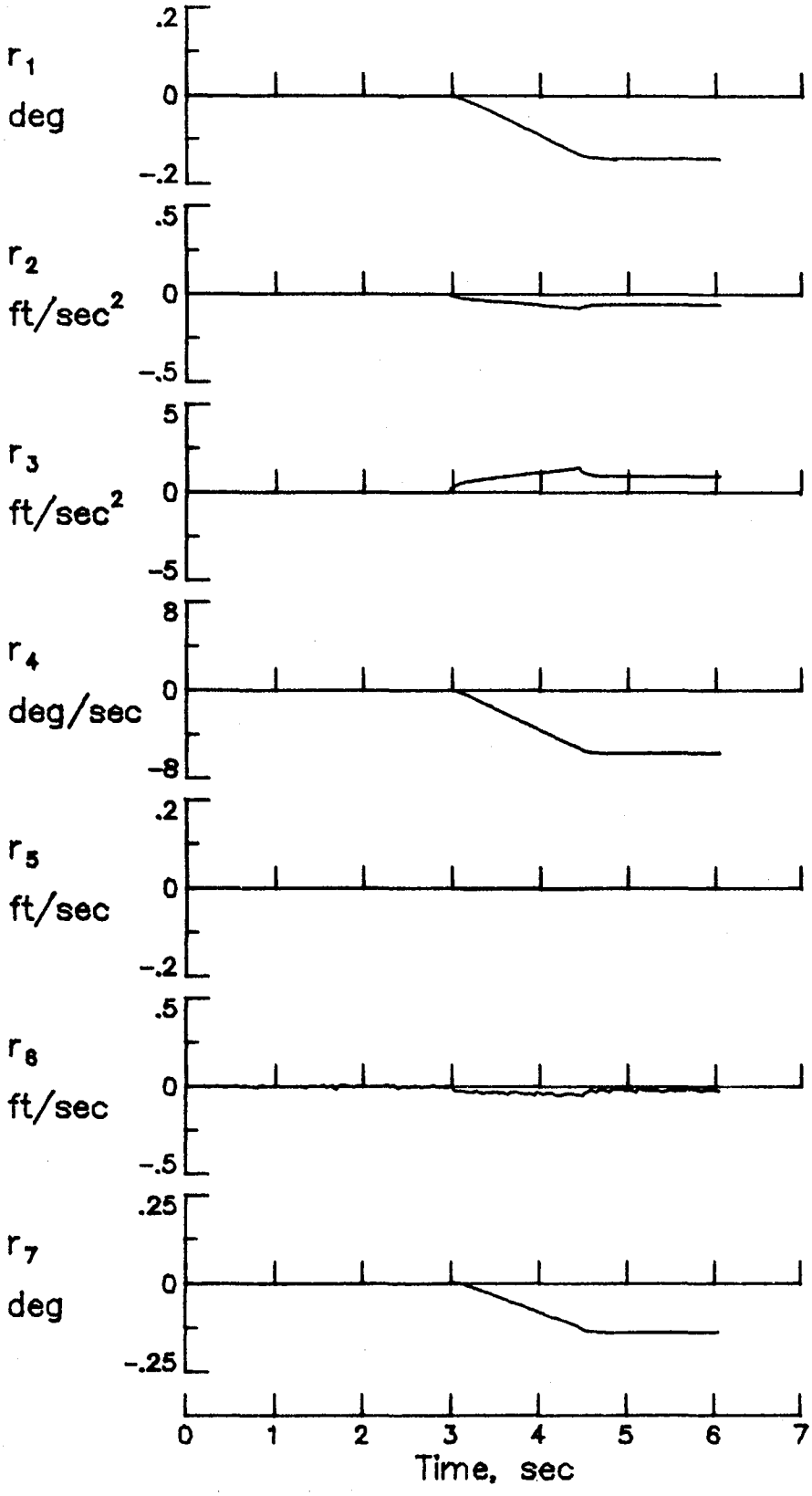

Figure 5.- Filter residuals for an 8 degree ramp spoiler failure with linear measurements.

1. Report No.	2. Government Accession No.	3. Recipient's Catalog No.
NASA TM-87576		

4. Title and Subtitle	5. Report Date
A Preliminary Evaluation Of A Failure Detection Filter for Detecting and Identifying Control Element Failures In A Transport Aircraft	July 1985
	6. Performing Organization Code 505-34-03-07
7. Author(s)	8. Performing Organization Report No.
W. Thomas Bundick	
9. Performing Organization Name and Address	10. Work Unit No.
NASA/Langley Research Center Hampton, VA 23665	11. Contract or Grant No.
	13. Type of Report and Period Covered Technical Memorandum
12. Sponsoring Agency Name and Address	14. Sponsoring Agency Code
National Aeronautics and Space Administration Washington, DC 20546	

15. Supplementary Notes

Programming support was supplied by Mrs. Jessie Yeager of Kentron International.

16. Abstract

The application of the failure detection filter to the detection and identification of aircraft control element failures has been evaluated in a linear digital simulation of the longitudinal dynamics of a B-737 Aircraft. Simulation results show that with a simple correlator and threshold detector used to process the filter residuals, the failure detection performance is seriously degraded by the effects of turbulence.

17. Key Words (Suggested by Author(s))	18. Distribution Statement
Failure Detection Failure Detection Filter Fault Detection Restructurable	Unclassified - Unlimited Subject Category - 08

19. Security Classif. (of this report)	20. Security Classif. (of this page)	21. No. of Pages	22. Price
Unclassified	Unclassified	84	A05

For sale by the National Technical Information Service, Springfield, Virginia 22161